Technical University of Denmark

DTU

Modeling and experimental testing activity of the Voltage Optimization Unit.

Testing activity of the distribution transformer with single-phase on-load tap changer in an experimental low voltage network and investigation of different control logics.

Zecchino, Antonio; Hu, Junjie; Marinelli, Mattia

Publication date:
2016

Document Version
Publisher's PDF, also known as Version of record

Link back to DTU Orbit

DTU Library
Technical Information Center of Denmark

Technical University of Denmark

DTU

Modeling and experimental testing activity of the Voltage Optimization Unit

Testing activity of the distribution transformer with single-phase on-load tap changer in an experimental low voltage network and investigation of different control logics

Febuary 2016

DTU Electrical Engineering
Department of Electrical Engineering

Modeling and experimental testing activity of the Voltage Optimization Unit,
Testing activity of the distribution transformer with single-phase on-load tap changer in an experimental low voltage network and inves-tigation of different control logics

Authors:
Antonio Zecchino
Junjie Hu
Mattia Marinelli

Department of Electrical Engineering
Centre for Electric Power and Energy (CEE)
Technical University of Denmark
Elektrovej 325
DK-2800 Kgs. Lyngby
Denmark

www.elektro.dtu.dk/cee
Tel: (+45) 45 25 35 00
Fax: (+45) 45 88 61 11
E-mail: cee@elektro.dtu.dk

SUMMARY

In the EUDP project 'Energy saving by voltage management' two reports are provided by Technical University of Denmark (DTU) covering the simulation studies and experimental work. The first report presented the simulation results regarding the technical evaluation of on-load tap changers in solving the voltage problems in presence of photovoltaic distributed generation, using Bistrup distribution grid (DONG Energy) as a test case.

This second report presents the experimental results of the testing activity of the Voltage Optimization Unit (VOU), i.e., a distribution transformer with single-phase on-load tap changers (OLTC) in an experimental low voltage grid. Both the transformer internal behavior and its effective operations under different unbalanced bidirectional power flow conditions have been investigated. Moreover, different control logics are analyzed based on their control objectives and control inputs, which include network currents and voltages that can be measured either locally or remotely. The experimental validation has been performed in the research infrastructure SYSLAB-PowerLabDK, a laboratory facility for the development and test of control and communication technology for active and distributed power systems, located at DTU Risø campus.

The experimental test validates the control performance of the OLTC transformer and the test indicates that, using remote measurement, the voltage of the system can be kept in a safe operational band. However, the remote measurement implies additional cost investments of to the system operator, thus a proactive tap algorithm is developed and tested in this project, relying on local measurements. In addition, we also compared the experimental result with the one simulated in the DigSilent PowerFactory software environment (the software used in the first report), and the results show that the system components have been properly modeled.

Note that the system tested in this report is a simplified network that cannot characterize all the features of a real distribution network, even though it is able to catch the most important ones. Future study could include two aspects: 1) investigate the OLTC's application in an active distribution network characterized by several subfeeders, where higher penetration of different distributed generations is present; and 2) combine the

OLTC control with smart-metering technology, where the measurements from the smart meters can be used as inputs for the control actions of the OLTC transformer.

TABLE OF CONTENT

ABBREVIATIONS

VOU: voltage optimization unit

OLTC: on-load tap changer

EV: electric vehicle

LDC: line drop compensation

CL: control logic

MV/LV: medium voltage/low voltage

DSO: distribution system operator

V2G: vehicle to grid

RMS: root mean square

1 INTRODUCTION

1.1 Background

With the increasing penetration of distributed and renewable energy resources connected to the distribution network, network operators are facing voltage-deviation problems, such as voltage rise introduced by non-programmable photovoltaic generation [1]–[3], or voltage drop, owing to the increasing number of electric vehicles and heat pumps [4],[5]. To address the voltage problems, instead of choosing expensive expansion investments, even though the capacities of the grid are far from exhausted, voltage control at the LV side of the MV/LV transformer by on-load tap changers (OLTC) is largely proposed in the literature [6]–[10].

In [6], an OLTC circuit is developed for use with a low-voltage transformer (10/0.4 kV, or equivalent), in which the tap position could be set independently for each low-voltage feeder. To model the low-voltage system and the control logic of OLTC, the author uses two simulation tools: Excel and Simulink. The controller takes the measurement from the far end of the feeder. If the far-end voltage is below the minimum limit, the control block increases the tap setting by one step. If the far-end voltage is above the maximum limit, the control block decreases the tap setting by one step. The results showed that the voltage could be kept within the limits. In [7], phase-wise OLTC is assessed technically in Flemish LV distribution grids. Compared to [6], the proposed tapping logic considers the influence of PV in terms of active power injection. The simulation is performed in DigSilent PowerFactory, and the results showed that the phase-wise OLTC partly eliminates the violations of both voltage limits and thermal constraints. However, voltage unbalances can increase owing to the independent tap-changing control per phase. In [8]–[10], the same authors investigated the capability of phase-wise OLTC, with the objective of evaluating the hosting capacity of a distribution network characterized by high PV penetration. In the studies, details regarding the modelling and control algorithms of the OLTC are presented. The simulations are performed in Digsilent Power-Factory. The results showed that the phase-wise OLTC can significantly improve the penetration of PVs, since it reduces phase-neutral voltage deviations from the rated value, with acceptable increases of the voltage unbalance factor.

However, the current studies [6]–[10] focus on simulation-based validation which means experimental-based validation is still largely missing in the field.

9

1.2   Objective

In this experimental activity part, four objectives are defined: 1) test the control performance of the phase-wise on-load tap-changer transformer and characterize the features of the OLTC transformer dynamics; 2) reproduce a typical Danish distribution system in a simplified experimental network;3) validate the simulation models used in the [first part](#) of the project using the experimental measurements; 4) examine three types of control logics of the phase-wise on-load tap-changer transformer in an experimental low-voltage network, considering the line-drop compensation technology.

1.3   Report structure

The experimental system is located in SYSLAB which is a laboratory facility for the development and test of control and communication technology for active and distributed power systems. The facility is spread across four sites at the DTU (Technical University of Denmark) Risø campus. Thus, all the experimental acitivities are performed in SYSLAB. To report this activity, the document is organized as follows:

In Chapter 2, the choice of the experimental system setup is justified in a way that it can represent the features of a real Danish low voltage distribution network. Further attention is given to a brief description of the involved components.

Chapter 3 presents the internally physical structure of the OLTC transformer as well as the dynamic response of the OLTC transformer in term of its reaction to voltage changes.

In Chapter 4, the open-circuit test and the on-load test are reported for a complete and exhaustive characterization of the OLTC transformer.

In Chapter 5, four kinds of control logics (CL) related to phase-wise OLTC are described.

Chapter 6 focuses on the evaluation of the real tap-changers activities and the implemented models. With the purpose of evaluating the modeled system, the results obtained from the practical tests are compared to the simulations' ones, by monitoring and calculating the same parameters and indexes.

In Chapter 7, the control performance of three control logics described in Chapter 5 is presented.

2 EXPERIMENTAL SYSTEM DESIGN AND OVERVIEW

In this Section, the choice of all the utilized components and the experimental system design is justified in a way that it can represent a real Danish low voltage distribution network. Further attention is given to a brief description of the involved components.

2.1 Setup specification through analysis of a real network

The physical setup utilized for the experiments has been built to reproduce as realistically as possible a reference real Danish LV distribution network, whose data have been provided by Dong Energy, a local DSO. The considered distribution system has already been adopted in the previously presented works dealing with the feasibility of the decoupled-tap-changer approach and its effect on the network ([8]–[10]). In order to define the size of the devices employed in the experimental setup (i.e., OLTC rated power, cable length and impedance, loads power), an analysis of the electrical characteristics of a real system is conducted, in particular with the aim of selecting a suitable cable size (length and section) to represent the line impedance of the reference network.

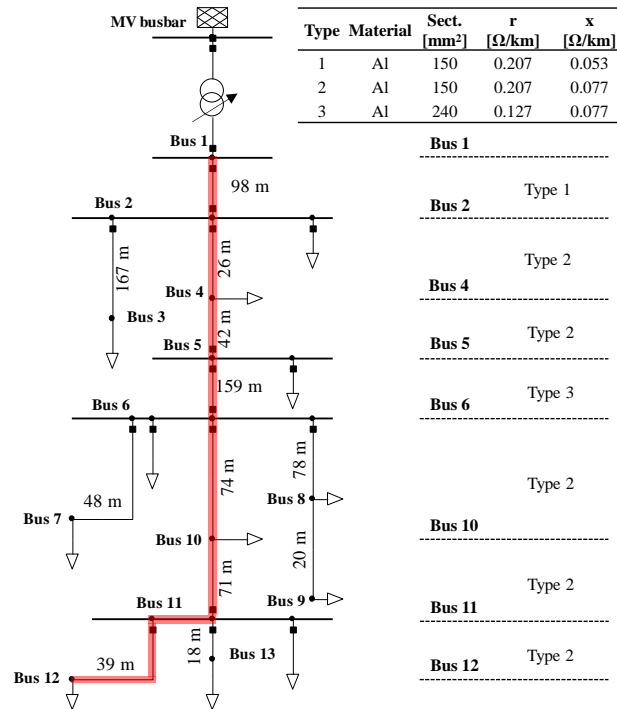| Type	Material	Sect. [mm²]	r [Ω/km]	x [Ω/km]
1	Al	150	0.207	0.053
2	Al	150	0.207	0.077
3	Al	240	0.127	0.077

Fig. 1. Danish real distribution feeder layout

11

In Fig. 1, the distribution feeder layout is shown, along with the cables length and imped-ance. In order to have a simplified setup, this analysis' aim is to calculate an equivalent impedance of the real network. Further, the line sections connecting the MV/LV trans-former and the farther busbar (i.e., Bus 12) were considered (highlighted in Fig. 1). The total impedance for the highlighted line is given by (1):

$$Z_{TOT} = \sum_{type=1}^{3} \left| z_{type} \right| \cdot L_{type} \tag{1}$$

where $z_{type} = |r_{type} + j\, x_{type}|$ is the per-unit-length impedance [Ω/km] and L_{type} is the total length [km], both associated to each cable type and section. The total impedance Z_{TOT} is then used to calculate an index of the 'impedance density' defined as the ratio between total impedance and total load power:

$$K_Z = \frac{Z_{TOT}}{P_{TOT}} \tag{2}$$

where P_{TOT} is the total load power [kW] calculated as the average consumption of the loads connected to the network, measured during one day operation, and K_Z is defined as 'impedance density' index [Ω/kW].
The line length for the experimental setup can now be defined through (3):

$$L_{TEST} = \frac{K_Z \cdot P_{TEST}}{z_{cable}} \tag{3}$$

where two of the variables need to be set in accordance with the test:

- P_{TEST}: OLTC's rated power [kW] (also defining the loads' size)

- Z_{cable}: impedance of the cable [Ω], depending on the type selected for the setup.

In this case, the impedance of the line highlighted in Fig. 1 is 92.64+j36.84 mΩ, while the average load power during one day operation of the network is 31 kW. These values resulted in an impedance density $K_Z = 3.22$ Ω/kW. In order to recreate the most realistic network equivalent, the closest size available for the OLTC device is 35 kW, while the cable chosen for the setup is a 16 mm^2 copper conductor (z_{type}=1.45+j0.081 Ω/km). With these values, the cable length can be calculated as for (3) resulting in 75.3 m.
To verify the accuracy of the analysis, an evaluation of the three-phase short-circuit current has been performed, by simulating a fault at Bus 12 in the real system's model and at the load bus in the equivalent circuit. They amounted respectively to 1626 A and 1638 A, thus validating the study.

2.2 Experimental setup

The experimental validation has been performed in the research infrastructure SYS-LAB-PowerLabDK, a laboratory facility for the development and test of control and communication technology for active and distributed power systems, located at the DTU Risø campus [11].

As result of the proposed analysis, the basic simplified experimental setup layout has been composed of the 35 kVA decoupled-phase OLTC transformer under investigation, a 16 mm^2 three-phase 75 meter-long copper cable and a resistive load with the feature of independent single-phase power absorption control up to 15 kW per phase.

In addition to the mentioned realistic passive outline, an EV featured with Vehicle-To-Grid (V2G) services provision has been connected to the system aiming at representing a single-phase active user connected to the LV grid. It allows grid support by raising the voltage locally, thanks to the possibility of active power injection.

The setup of the experiment is schematically depicted in Fig. 2 and Fig. 3. It can be noticed that two measurement devices have been utilized for monitoring and collecting data. Specifically, they have been installed at the two terminals of the cable, i.e., at the secondary side of the OLTC and at the load/EV bus. In particular, they allow monitoring voltages and currents on the four active wires (the three phases and the neutral conductor) at the two measurement points, both in terms of root-mean-square (RMS) values and of sequence-related indexes. The utilized measurement devices are two 'ELSPEC BlackBox G4500 Power Quality Analyzer' units [12].
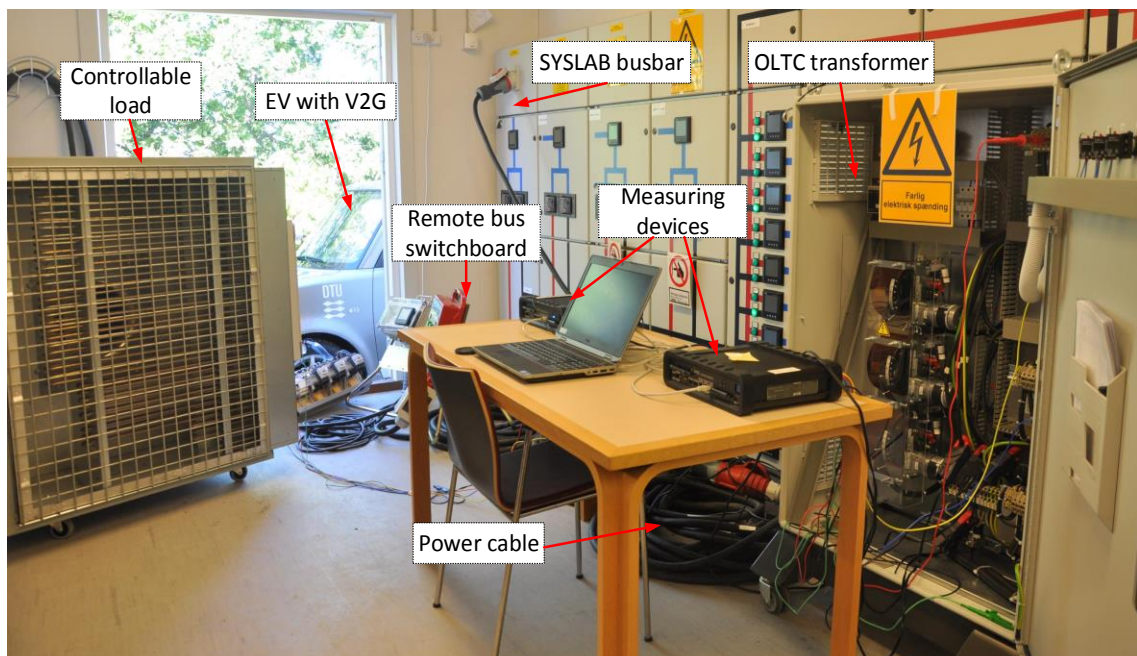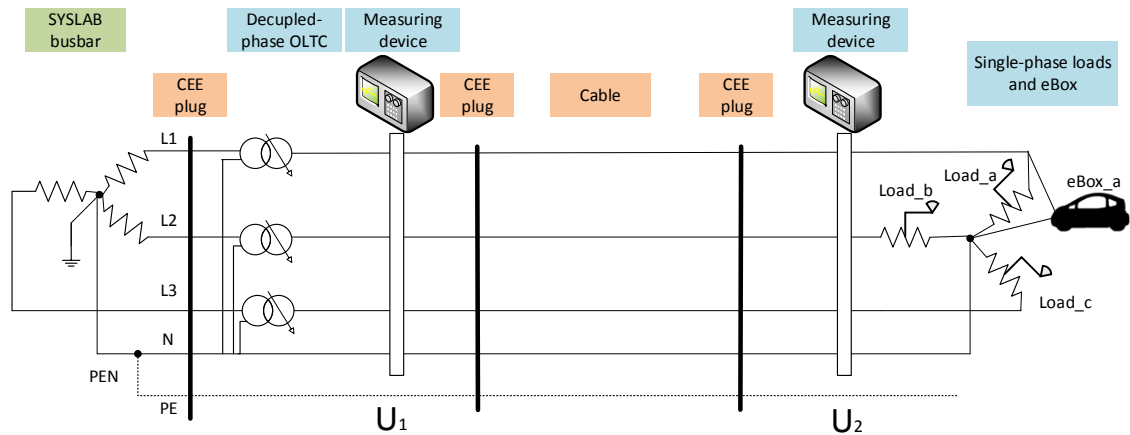

Fig. 2. Experimental setup layout

Fig. 3. Schematic system layout for the experimental activities

2.3 Controllable load

As discussed in Paragraph II-B, a custom-made 45 kW (i.e., 15 kW per phase, adjustable with steps of 0.1 kW) load unit equipped with a three-phase CEE 63 A plug for the supply has been utilized (Fig. 4). According to the active power independently settable on each phase through a touchscreen interface, appropriate connections of internal resistor branches are provided, so to achieve the necessary resistance, resulting in the desired active power absorption. It is therefore clear that the load is representable with a constant-impedance model, with reference to the ZIP theory [13]. In fact, the unit is manufactured so the set active power P_0 corresponds to the effectively absorbed power P_{eff} just under nominal voltage conditions V_0. Otherwise the effective load power would change with the square of the ratio of the effective supply voltage V_{eff} and the rated one, as in (5).

$$P_{eff} = P_0 \cdot (V_{eff}/V_0)^2 \tag{5}$$

Fig. 4. Phase-independently controllable resistive load and the control interface

2.4 Electric vehicle

The utilized EV is an eBox, a conversion of a Toyota Scion xB vehicle into a battery electric vehicle produced by the U.S. Company AC Propulsion (Fig. 5). The eBox is equipped with a 35 kWh battery and a power electronics unit (PEU) capable of single-phase bidirectional power transfer up to 20 kW. It is controllable either by the EV computer that interfaces with the PEU using build-in vehicle smart link (VSL) or directly via the vehicle management system (VMS) [14].

In this case, the VMS has been utilized. It allows the manual adjustment of the injected/absorbed current – limited to 16 A due to the technical limitation of the single/three-phase switchboard, which the EV is connected to. Therefore, for the performed experimental tests, the set current has been considered as reference value for the analysis of the operative scenarios. Again with reference to [13], the EV is representable with a 'constant-current' model, meaning that its behavior is characterized by a constant ratio of active power and voltage. Therefore it is clear that, unless the operation is run under nominal voltage condition, the injected power P_{eff} would deviate from the nominal power P_0 with the ratio of the effective supply voltage V_{eff} and the rated voltage V_0, according to (6).

$$P_{eff}=P_0 \cdot (V_{eff}/V_0) \tag{6}$$

Fig. 5. eBox connected to the ending terminal of the line through a single-phase switchboard

2.5 Cable impedance calculation

For the calculation of the cable impedance, two methods are proposed: deriving complex equations considering the voltage drop along the cable or relying on a regression method.

The first approach allows the calculation of the resistance of the cable by measuring the voltage at the two terminals of the cable and the current flowing through. By taking the phase angles into account, it is also possible to calculate the reactance of the cable. Considering phasors, the voltages at the two ending terminals of the cable have different magnitude and angles, whereas, as the system is a LV system, the current in each end has same magnitude and angle. The following equations consider complexes representations of current and voltages, where the subscript 1 and 2 indicate the starting and ending terminals of the line, respectively.

$$\overline{\Delta V} = \bar{V}_1 - \bar{V}_2 = \bar{I} \cdot \bar{Z} = \bar{I} \cdot (R + jX) \tag{7}$$

$$\begin{cases} R = \Re\mathrm{e}(8) = \frac{V_1(\cos\varphi_1)}{I} - \frac{V_2(\cos\varphi_2)}{I} \\ X = \Im\mathrm{m}(8) = \frac{V_1(\sin\varphi_1)}{I} - \frac{V_2(\sin\varphi_2)}{I} \end{cases} \tag{8}$$

Utilizing the test setup described in the previous Section, the following procedure has been followed:

Set the dumpload power to 1 kW.

- Wait 5 minutes, in order to get an averaged value.
- Increase the power by 1 kW.
- Wait 5 minutes.
- Continue until 11 kW has been reached

Actual power levels and 5 minute averages of the measurements can be seen in Table 1.

Table 1. Measurements for reactive power calculations

P [kW]	1.16	2.26	3.37	3.81	4.49	5.57	6.65	7.76	9.25	10.67	11.33
I [A]	4.96	9.73	14.50	16.42	19.39	24.17	28.89	33.71	40.38	46.66	49.56
V_1[V]	233.52	233.44	233.71	233.67	233.60	233.24	233.19	233.86	233.50	234.08	234.27
V_2[V]	232.95	232.34	232.04	231.78	231.36	230.44	229.85	229.92	228.78	228.59	228.40
φ_1 [rad·10^{-3}]	22.78	20.89	20.15	19.77	19.24	18.77	18.62	18.75	18.97	19.80	20.27
φ_2[rad·10^{-3}]	23.42	22.04	21.32	20.76	20.43	20.17	20.21	20.52	21.34	22.51	23.21

The linear regression is a first order equation (equation (9)) where two fitted parameters, α and β, influence the argument in order to give a linear output. The two parameters

have been calculated from existing arguments and output values, using the MatLab functions *polyval* and *polyfit*.

$$y = \alpha x + \beta \tag{9}$$

The argument *x* is the actual power and output *y* is the impedance per km.

The imaginary calculations at low currents, i.e. the first three power levels, are imprecise and unrealistically high reactance has been obtained; these values have therefore been ignored when linearising. The linearisation parameters are shown in Table 2.

Table 2. Linear regression parameters

	A	*B*
R	0.005195494895876	1.518473715004860
X	-0.001160472207781	0.156054586447325

Datasheet values for the impedance are taken into account in order to compare the accuracy of the calculated impedance. Units in the datasheet are expressed in ω/km, thus the calculated impedance has been scaled up.

In Fig. 6, the calculated impedance values are marked by 'x', the linearisation values are represented by the dashed lines and the datasheet values by the full lines. The reactance (red) is relatively constant across the power levels, and is close to the datasheet value. A possible reason for the slightly higher reactance could be that the cables are rolled up in order to save space. When a cable is rolled up it is similar to a coil and therefore works as an inductor. The cables are not magnetically sealed. The resistance (blue), shows a rather peculiar trend: it is increasing with each increasing power level, unlike the constant datasheet value.
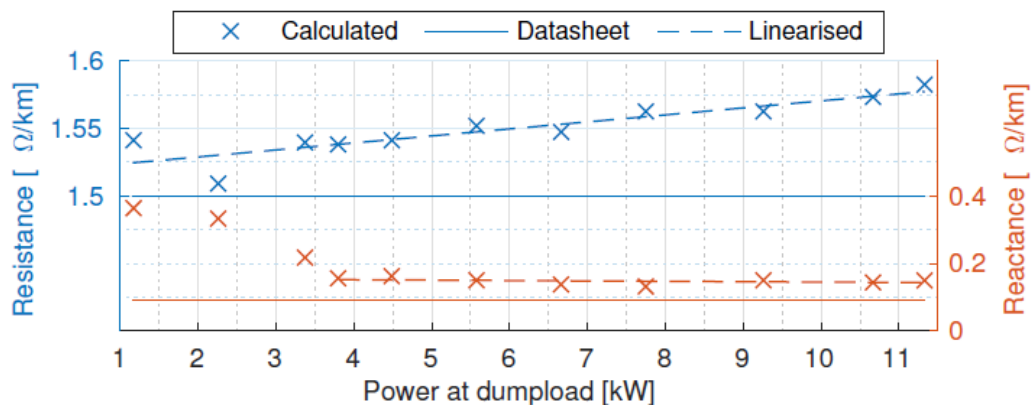

Fig. 6. Calculated, linearised and datasheet values for resistance and reactance

3 UNDERSTANDING THE FUNCTIONS OF THE VOU

3.1 VOU internal structure investigation

The VOU (a decoupled-phase OLTC transformer) under examination is a three-phase Delta-Wye transformer with the neutral grounded at the secondary side. Independently on each phase, it allows a regulation of the output voltage of ±10 % of the rated voltage V_n (400/230 V for either side). The rated power is 35 kVA, which corresponds to 11.66 kVA for each single-phase unit, while the rated current amounts to 50 A.

The peculiarity of the VOU is the capability of performing tap actions in three independent ways on the three phases, thanks to three different servo motors controlled by three independent control systems. The internal structure is reported in the picture of Fig. 7, where all the inner components are highlighted and named.
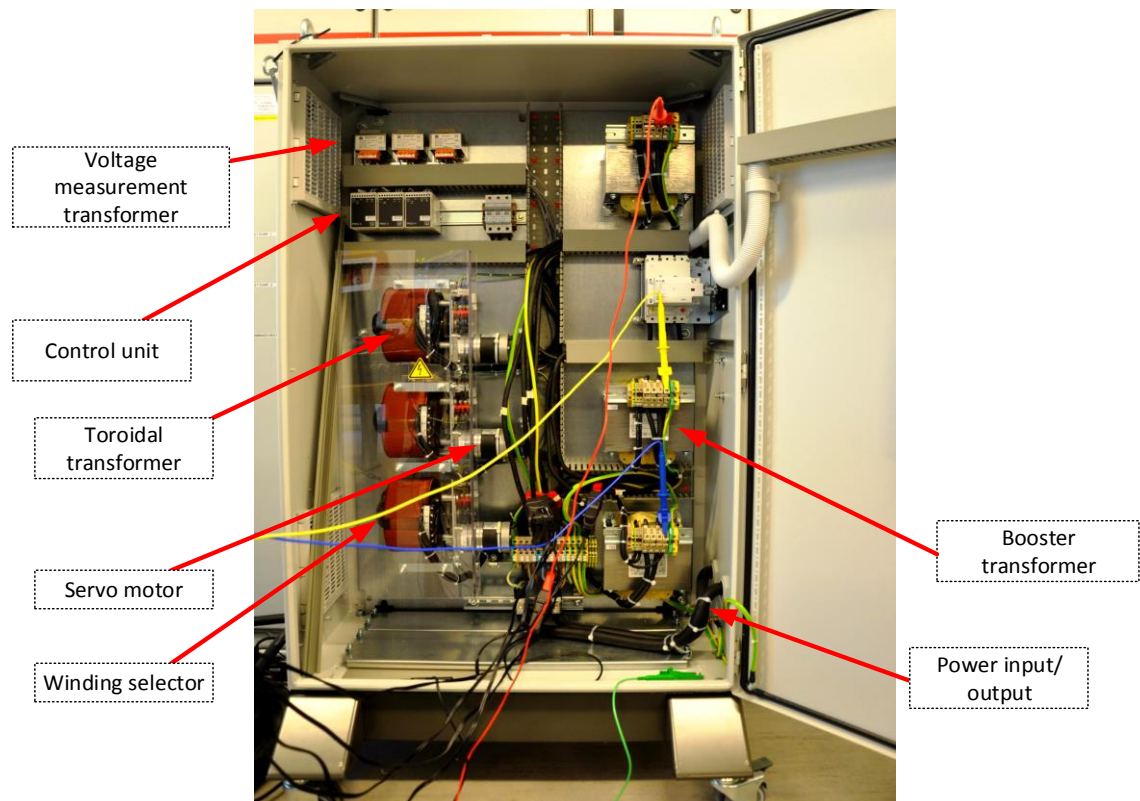

Fig. 7. VOU internal structure

It is composed by three single-phase toroidal coil transformers equipped with winding selectors connected to three servo motors, whose operations are managed by independent control units according to voltage measurements at the secondary side, obtained through three single-phase voltage measurement transformers. On the right side, three single-phase booster transformers are placed, whose main function is to split the total power among two steps of transformation, so to reduce the size of the three servo motors.

In the following figures (Fig. 8-14), detailed pictures of all the inner components of the transformer are reported.

Fig. 8. Power Circuit Breaker

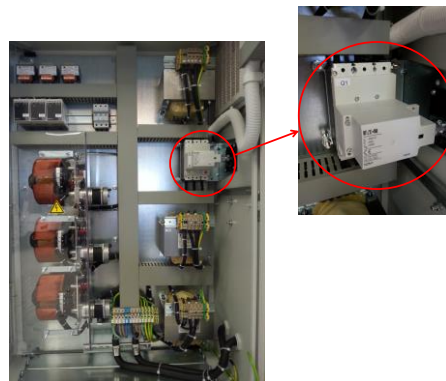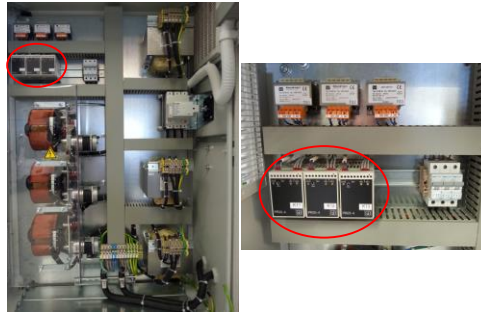Fig. 9. Control Circuit Breaker

Fig. 10. Control Unit

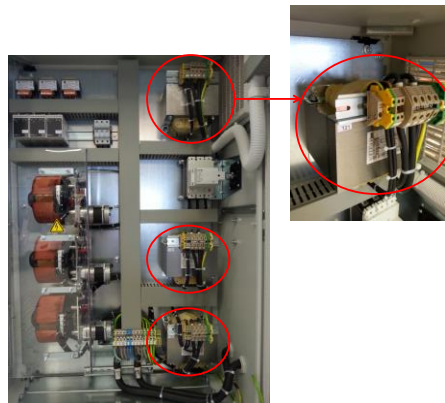Fig. 11. Three single-phase Measurement Transformers

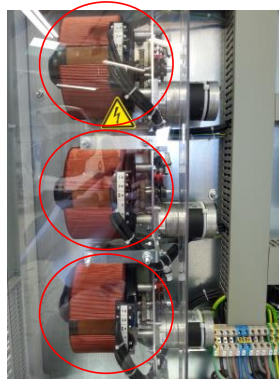Fig. 12. Three single-phase Booster Transformers

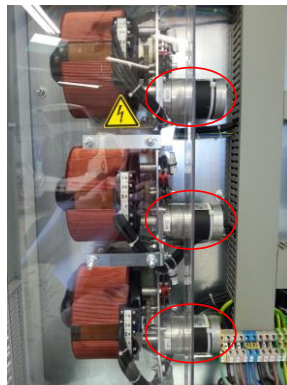Fig. 13. Three single-phase Variable Toroidal Transformers

Fig. 14. Three Servo Motors

The scheme in Fig. 15 highlights the two main circuits of the transformer: the power and control circuits.
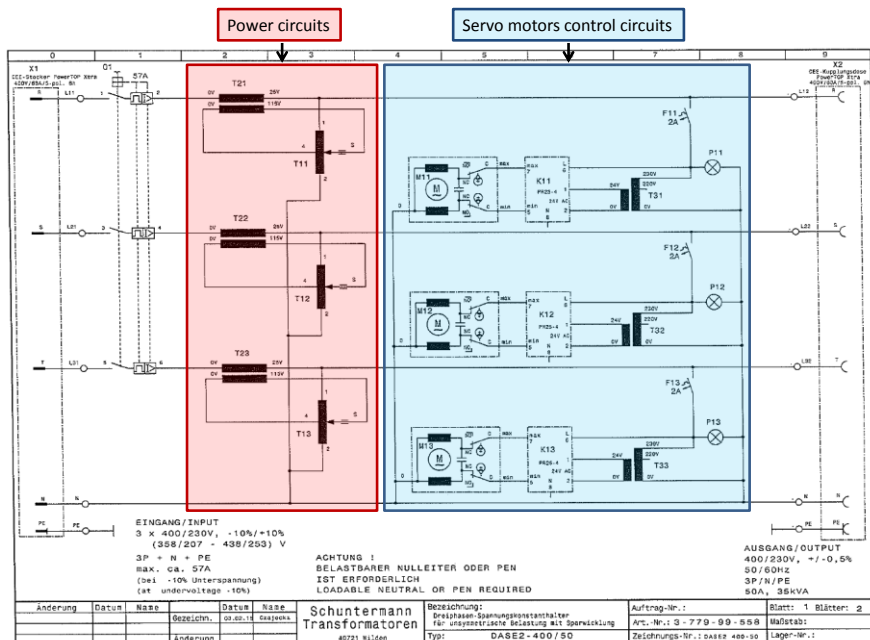
Fig. 15. Power and control circuits

3.2 Control mechanism and Tap-changing mechanism

This section presents the first practical activity: some simple preliminary tests have been performed with the aim of investigating the control behavior of the VOU.

Basically, the OLTC operates on a closed loop control. Independently on each phase, the output voltage is measured and compared with a reference voltage in the control unit. Whenever it exceeds the allowed dead band (1 % of V_n), tap actions are performed until the dead band is reached again.

Firstly, the tap operation scheme depicted in Fig. 16 has been considered as a reference.
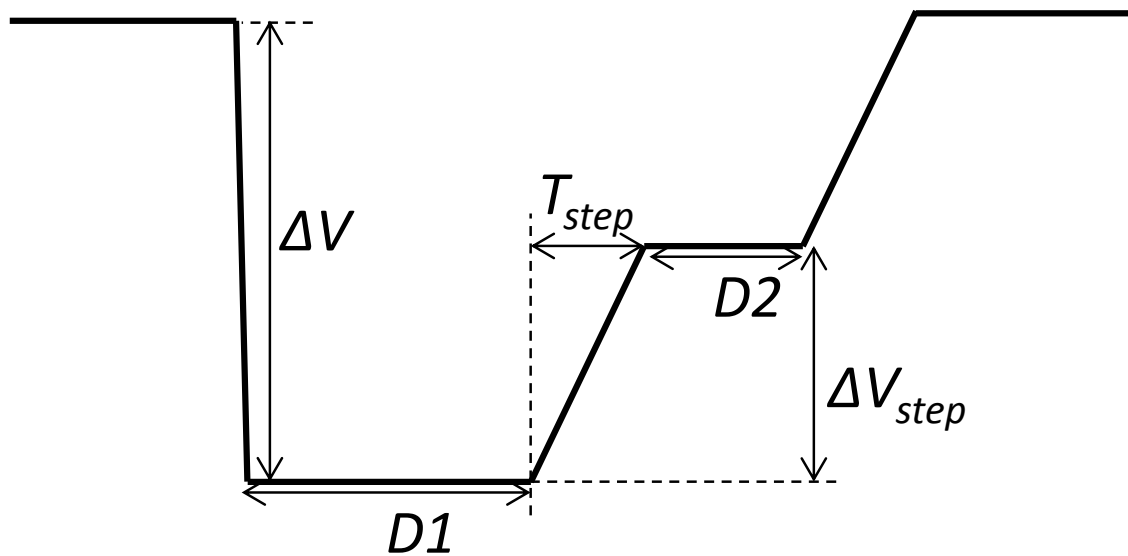
Fig. 16. Reference OLTC tap operation

The tap action can be described as follows:

1. Due to the increase of the load on one phase, the voltage on that phase drops (ΔV);

2. A delay-time *D1* prevents tap actions due to short-term voltage variations;

3. After the delay-time *D1* the voltage increases (ΔV_{step}), due to a tap action, which lasts T_{step};

4. Between two consecutive steps, a certain delay-time *D2* has been detected.

3.2.1 Preliminary Tests Results

Since the main objective was the determination of the parameters that characterize the physical tap action operation, it has been decided to monitor and analyze the RMS values of the phase-neutral voltages at the secondary side of the VOU while performing load steps. In order to obtain voltage drops that could cause a correspondent tap action, several load changings have been performed during a 25 minute-long time slot, named evnet #1 – event #4, as described in Table 3.

Table 3. Single-phase active power absorption after each event*

02 June 2015	Phase a [kW]	Phase b [kW]	Phase c [kW]
11:25	1/1.1	1/1.1	1/1.1
11:30 (event #1)	3/3.4	3/3.4	3/3.4
11:35 (event #2)	6/5.6	6/5.6	6/5.6
11:40 (event #3)	9/9.3	9/9.3	9/9.3
11:45 (event #4)	12/11.6	12/11.6	12/11.6

*Note: the first active power value is the one that has been manually set at the controllable load, the second one is the one that is effectively set by the load (according to some fixed combinations of resistances that that allow an active power absorption as close as possible to the one that is manually set under nominal voltage conditions). This difference is due to a not perfect calibration of the control unit, which therefore needs to be adjusted in the future.

Fig. 17 shows the three phase-neutral voltages at the secondary side of the trasmormer during the 25 minute-long time slot considered for the investigation of the tap behavior.
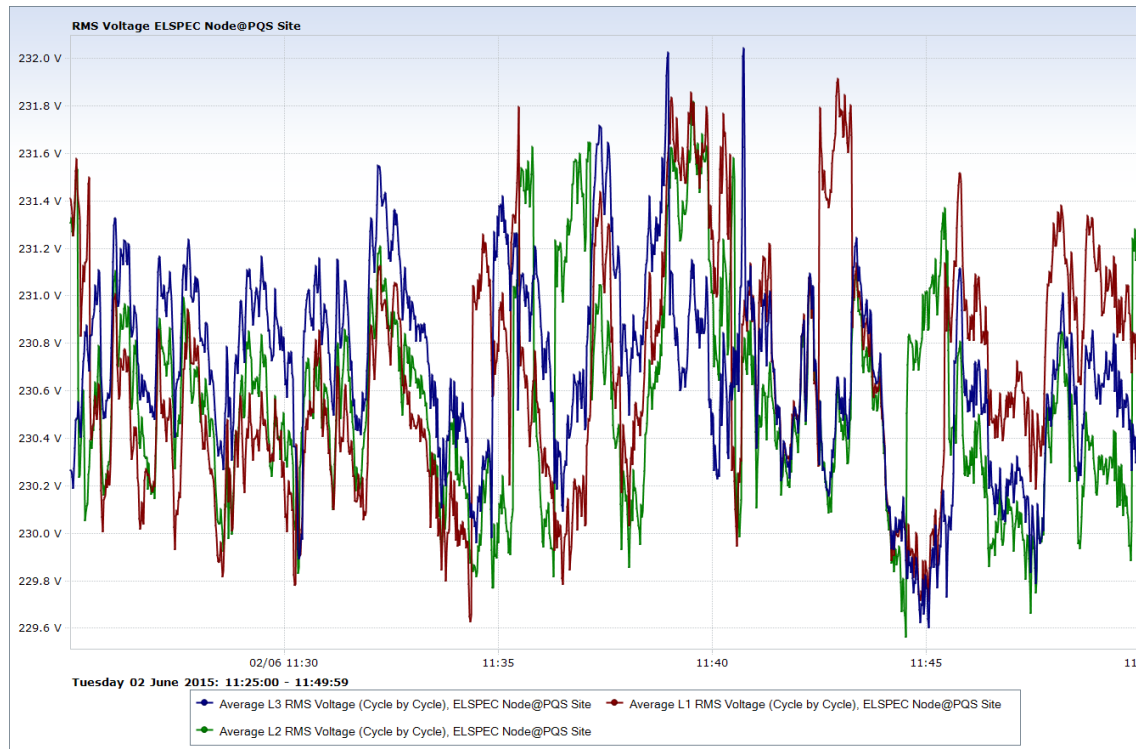
Fig. 17. Va, Vb and Vc trends between 11:25:00 and 11:49:59

In the following part, details of the measured voltages are reported. Specifically, for each event (load step – as described in Table 3), a general figure with its effects on the voltages precedes detailed zoomed-in figures for the analysis of the tap action and for the determination of the parameters afore defined.

<u>Event #1</u>

Fig. 18. 11:30 – Event #1: phase-neutral voltages on the three phases

As expected, from _{Fig. 18} (event #1) it is noticed that:
- Because of the increase of the load, the three voltages drop (ΔV);
- After a certain delay-time ($D1$) voltages increase, due to the tap actions;
- Each tap action lasts a certain time (T_{step});
- Between one tap action and the next one there is a certain delay ($D2$), which is not constant;
- Also the voltage raise due to the tap action (ΔV_{step}) is not constant.
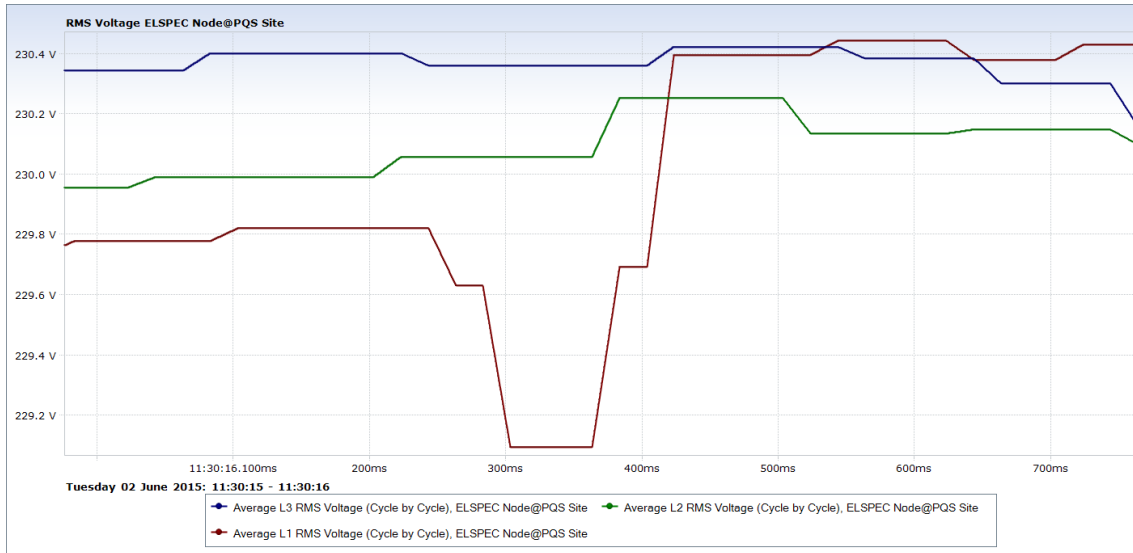
Fig. 19. 11:30 – Event #1: zoom-in of the phase-neutral voltage on phase a

Fig. 19 outcome:

$D1$ = 60 ms;

T_{step} = 20 ms;

$D2$ = 20 ms;

ΔV_{step_1} = 0.60 V − ΔV_{step_2} = 0.70 V
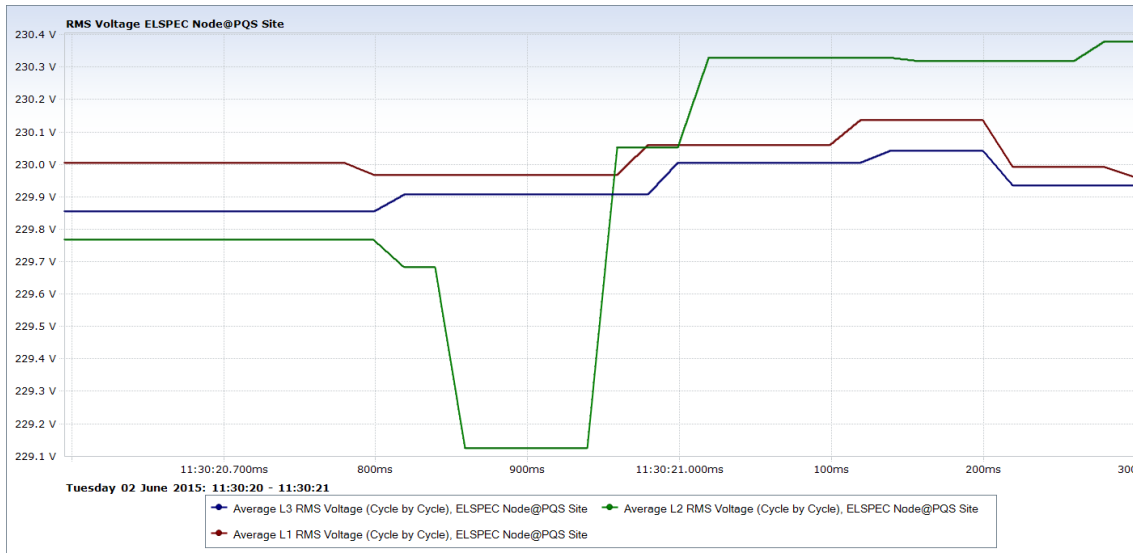
Fig. 20. 11:30 – Event #1: zoom-in of the phase-neutral voltage on phase b

Fig. 20 outcome:

$D1$ = 60 ms;

T_{step} = 20 ms;

($D2$ = 40 ms);

ΔV_{step_1} = 0.93 V − (ΔV_{step_2} = 0.27 V)

Fig. 21. 11:30 – Event #1: zoom-in of the phase-neutral voltage on phase c

Fig. 21 outcome:

$D1$ = 60 ms;

T_{step} = 20 ms;

$D2\_1 = D2\_2$ = 20 ms;

$\Delta V_{step}\_1 = 0.44$ V $- \Delta V_{step}\_2 = 0.51$ V $- \Delta V_{step}\_3 = 0.44$ V.

Event #2
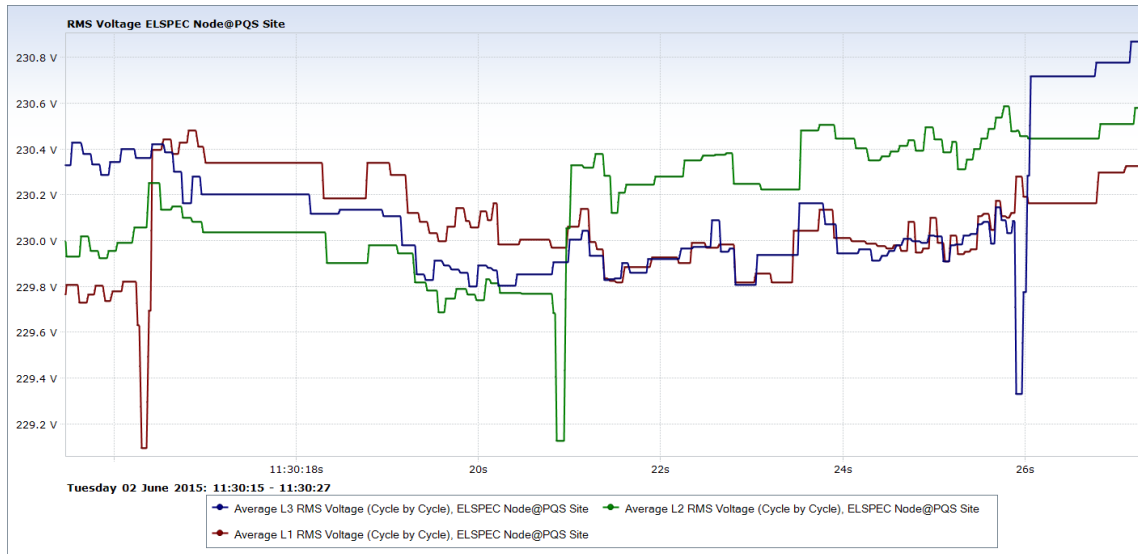

Fig. 22. 11:35 – Event #2: phase-neutral voltages on the three phases

From Fig. 22 (event #2) it is noticed that:

- Because of the increase of the load, the three voltages drop (ΔV);
- The voltage at phase c, although it drops, does not decrease so much to need to be raised up by a tap action – its zoom-in is not reported.
- After a certain delay-time (*D1*) voltage b increases, due to the tap actions;
- The voltage at phase a does not increase immediately, instead it increases only after achieving a sufficiently low value;
- Each tap action lasts a certain time (T_{step});
- Between one tap action and the next one there is a certain delay (*D2*), which is not constant;
- Also the voltage raise due to the tap action (ΔV_{step}) is not constant.

Fig. 23. 11:35 – Event #2: zoom-in of the phase-neutral voltage on phase a

Fig. 23 outcome:

$D1$ = 60 ms;

T_{step} = 20 ms;

$D2\_1$ = 20 ms – $D2\_2$ = 20 ms;

ΔV_{step}_1 = 0.32 V – ΔV_{step}_2 = 0.58 V – ΔV_{step}_3 = 0.59 V.

Fig. 24. 11:35 – Event #2: zoom-in of the phase-neutral voltage on phase b

Fig. 24 outcome:

$D1 = 160$ ms;

$T_{step} = 20$ ms;

$D2 = 40$ ms;

$\Delta V_{step\_}1 = 0.71$ V $- \Delta V_{step\_}2 = 0.86$ V.

Event #3
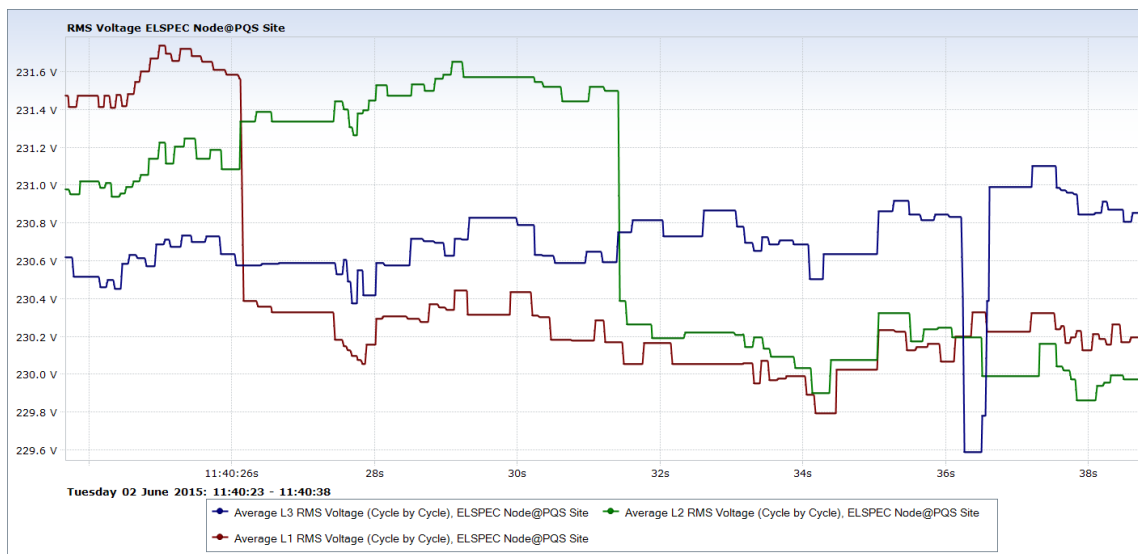
Fig. 25. 11:40 – Event #3: phase-neutral voltages on the three phases

From _{Fig. 25} (event #3) it is noticed that:

- Because of the increase of the load, the three voltages drop (ΔV);
- Voltages at phases a and b, although they drop, do not decrease so much to need to be raised up by a tap action – their zoom-ins are not reported
- After the delay-time ($D1$) voltage c increases, due to the tap actions;
- Each tap action lasts a certain time (T_{step});
- Between one tap action and the next one there is a certain delay ($D2$), which is not constant;
- Also the voltage raise due to the tap action (ΔV_{step}) is not constant.
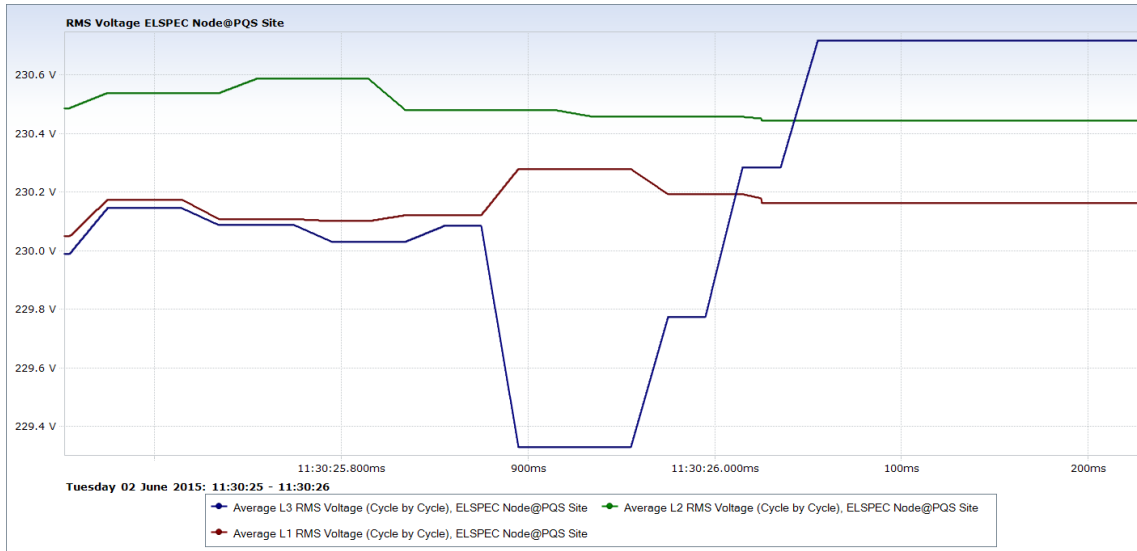

Fig. 26. 11:40 – Event #3: zoom-in of the phase-neutral voltage on phase c

_{Fig. 26} outcome:

($D1$ = 240 ms);

T_{step} = 20 ms;

$D2\_1$ = 40 ms – $D2\_2$ = 20 ms;

(ΔV_{step}_1 = 0.19 V) – ΔV_{step}_2 = 0.60 V – ΔV_{step}_3 = 0.61 V
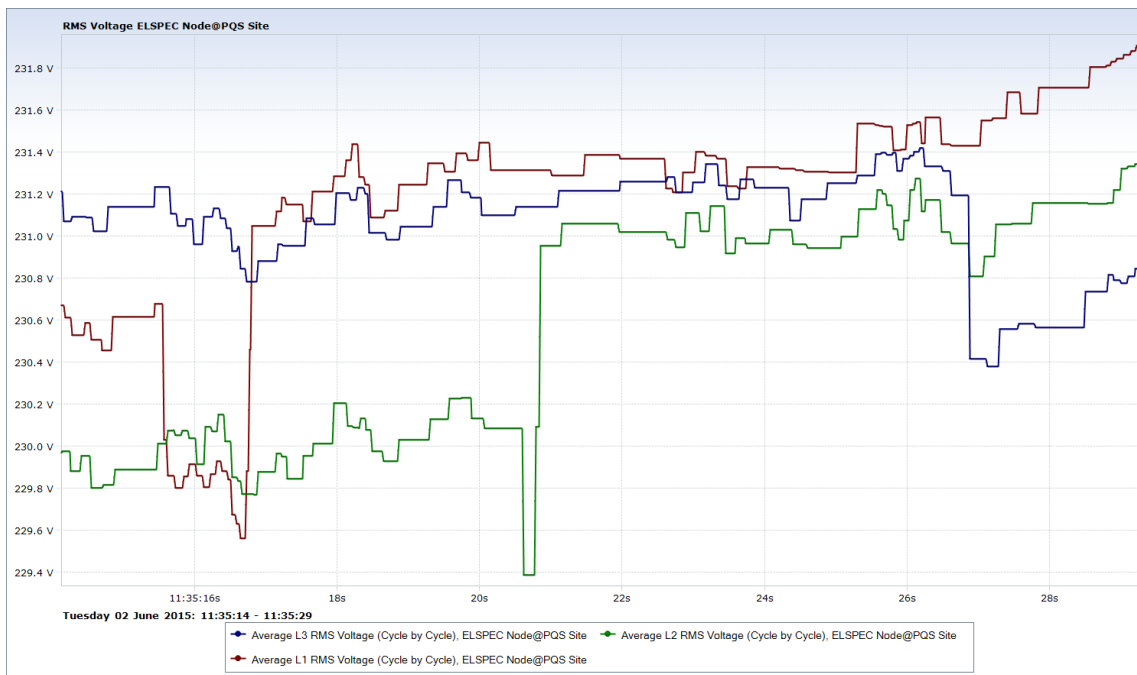
Event #4
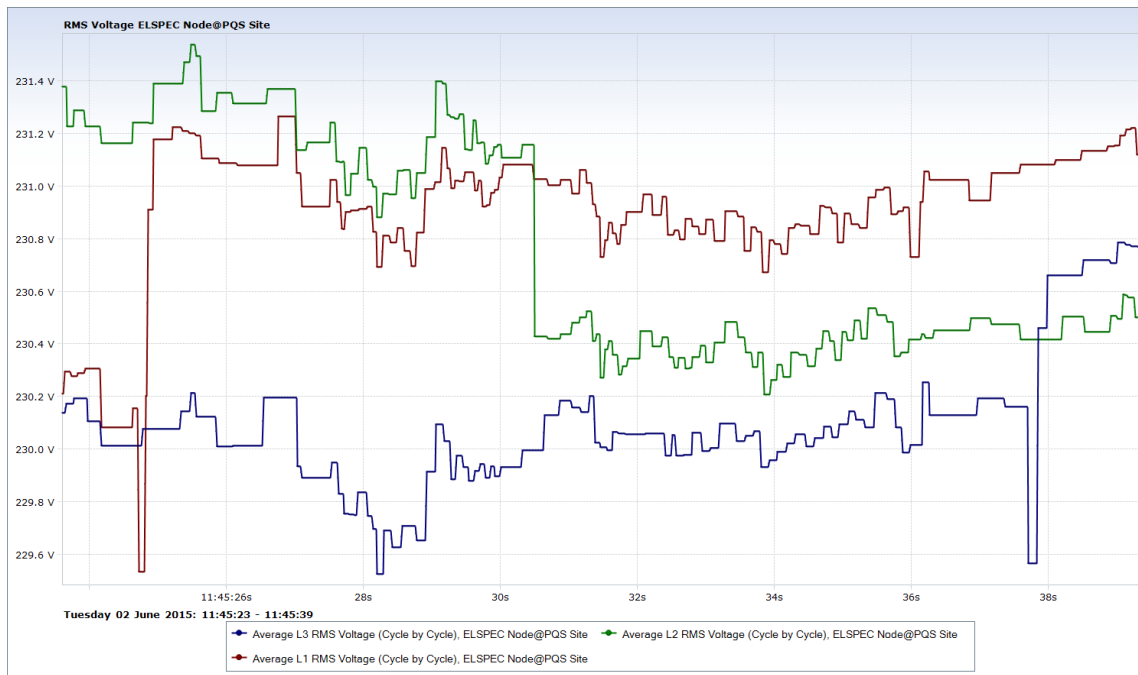
Fig. 27. 11:45 – Event #4: phase-neutral voltages on the three phases

From Fig. 27 (event #4) it is noticed that:
- Because of the increase of the load, the three voltages drop (ΔV);
- Voltage at phase b, although it drops, does not decrease so much to need to be raised up by a tap action – its zoom-in is not reported
- After the delay-time ($D1$) voltages a and c increase, due to the tap actions;
- Each tap action lasts a certain time (T_{step});
- Between one tap action and the next one there is a certain delay ($D2$), which is not constant;
- Also the voltage raise due to the tap action (ΔV_{step}) is not constant.
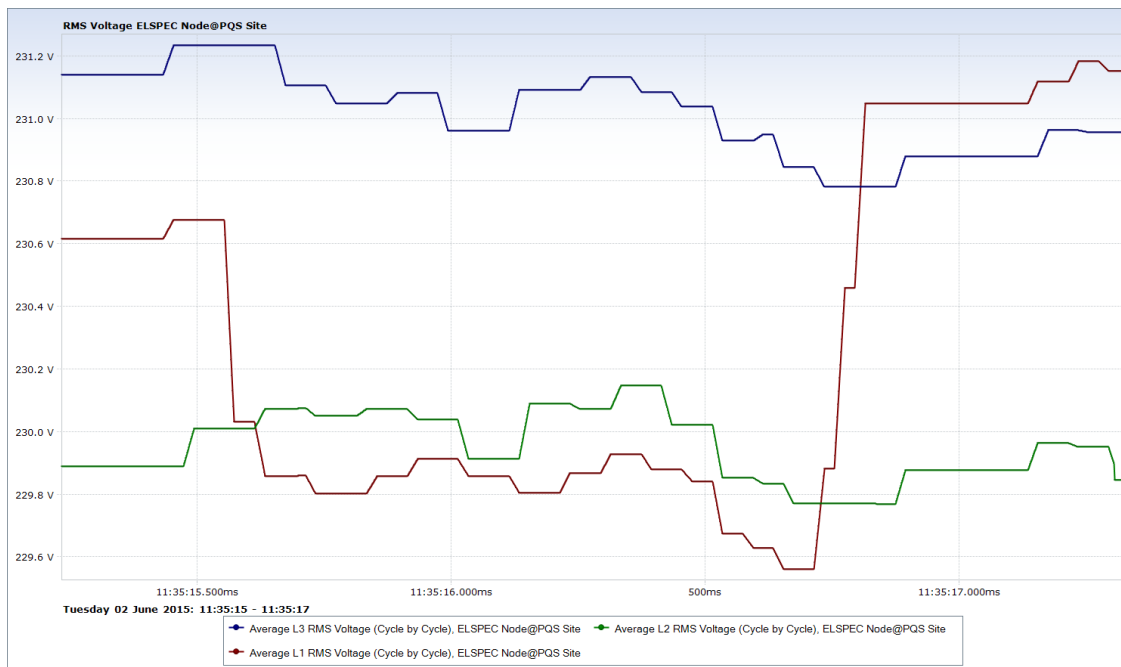
Fig. 28. 11:45 – Event #4: zoom-in of the phase-neutral voltage on phase a

Fig. 28 outcome:

$D1$ = 80 ms;

T_{step} = 20 ms;

$D2$ = 20 ms;

$\Delta V_{step\_}1$ = 0.67 V $- \Delta V_{step\_}2$= 0.71 V.

Fig. 29. 11:45 – Event #4: zoom-in of the phase-neutral voltage on phase c

Fig. 29 outcome:

$D1$ = 120 ms;

T_{step} = 20 ms;

($D2$ = 120 ms);

$\Delta V_{step\_}1$ = 0.89 V $-$ ($\Delta V_{step\_}2$ = 0.20 V).

Results Analysis and Interpretation

It has been noticed that the step ΔU related to the tap action is not constant: it assumes values within the range 0.3 V and 0.9 V.

The main reason is probably related to the supply voltage, which could be fluctuating during the step time (T_{step} = 20 ms), causing the modification of ΔV_{step}.

Considering this, it has been decided to proceed with further preliminary tests with the aim of verifying the reasons of such an inconstancy of ΔV_{step}, and of finding out its real value as well.

Thanks to this further investigation, it will be possible to obtain the real value of ΔV_{step} that will be applied to the PowerFactory model of the VOU, in order to reproduce its real behavior.

ΔV_{step} is not the only one parameter that assumes different values: also the delay-times $D1$ and $D2$ are not always constant. The delay-time $D1$ assumes values within the range 60 ms and 160 ms, while $D2$ within the range 20 ÷ 40 ms.

At any rate it is important to underline that the sampling time of the ELSPEC measurement device is 20 ms.

Overall results:

$D1 = 60 \div 160$ ms

$T_{step} = 20$ ms

$D2 = 20 \div 40$ ms

$\Delta V_{step} = 0.3 \div 0.9$ V

Mean values of the voltages between 11:25 and 11:49

Va = 230.66 V

Vb = 230.56 V

Vc = 230.69 V

➔ They could be considered as the voltage setpoints, i.e. the voltage that is considered as reference point by the controllers.

Tap actions:

If Va ≤ 229.6 V or Va ≥ 231.8 V ➔ TAP

If Vb ≤ 229.6 V or Vb ≥ 231.8 V ➔ TAP

If Vc ≤ 229.7 V or Vc ≥ 232 V ➔ TAP

➔ **Dead Band ≈ 2.3 V ; <u>Vsetpoint -1.15 V ÷ Vsetpoint +1.15 V</u>**

➔ **Dead Band ≈ 1 % Vn (± 0.5 % Vn)**

3.2.2 Correlation between ΔV_{step} and the supply voltage

As already said, since the voltage variation related to each automatic OLTC step operation is not always constant, it has been decided to investigate the existence of any correlation between the voltages at the two sides of the transformer.

In order to perform this investigation, two ELSPEC units have been utilized: ELSPEC "DTU 2" has been installed at the primary side and ELSPEC "DTU 1" at the secondary side. Their measurements are reported in the upper and botton upper voltage trends in Fig. 30-32.

The OLTC operations have been obtained through an increase of the load of 3 kW simultaneously on the three phases, precisely from 6 (6.1) kW to 9 kW.
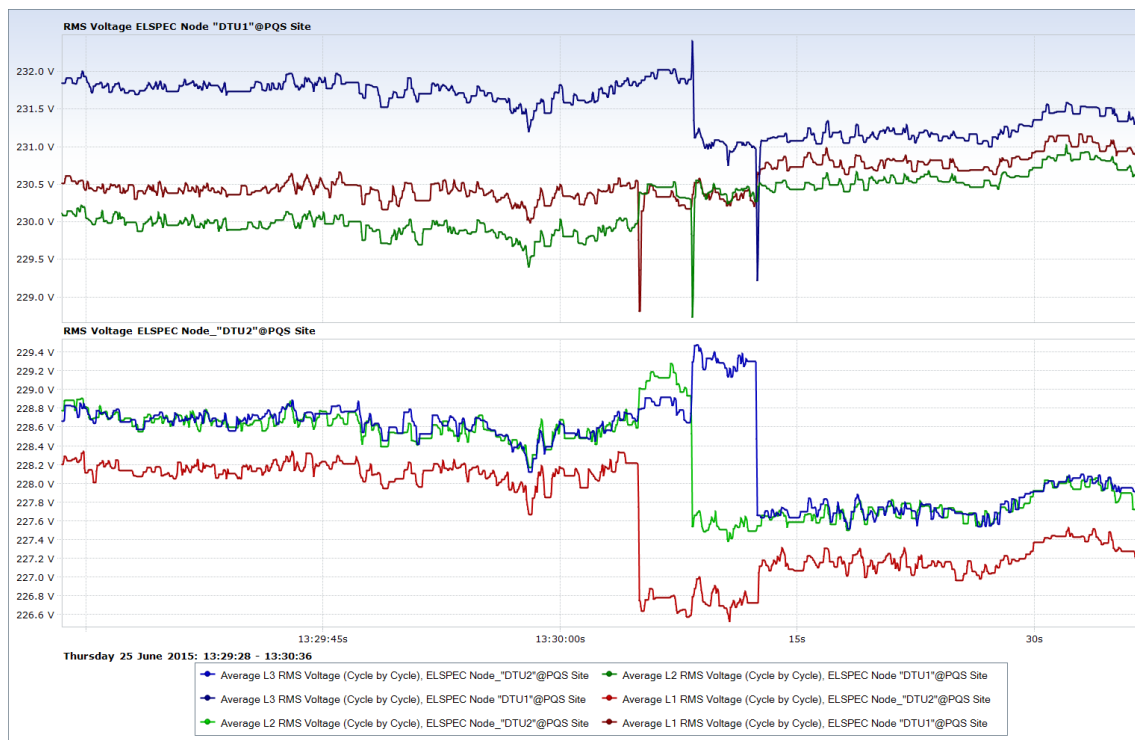
Fig. 30. Phase-neutral voltages on the three phases at the two sides of the transformer

Fig. 31. Zoom-in of the phase-neutral voltage on phase a

Fig. 31 outcome:

$\Delta V_{step\_}1 = 0.54$ V

$\Delta V_{step\_}2 = 0.79$ V

$\Delta Vprim = 0.10$ V
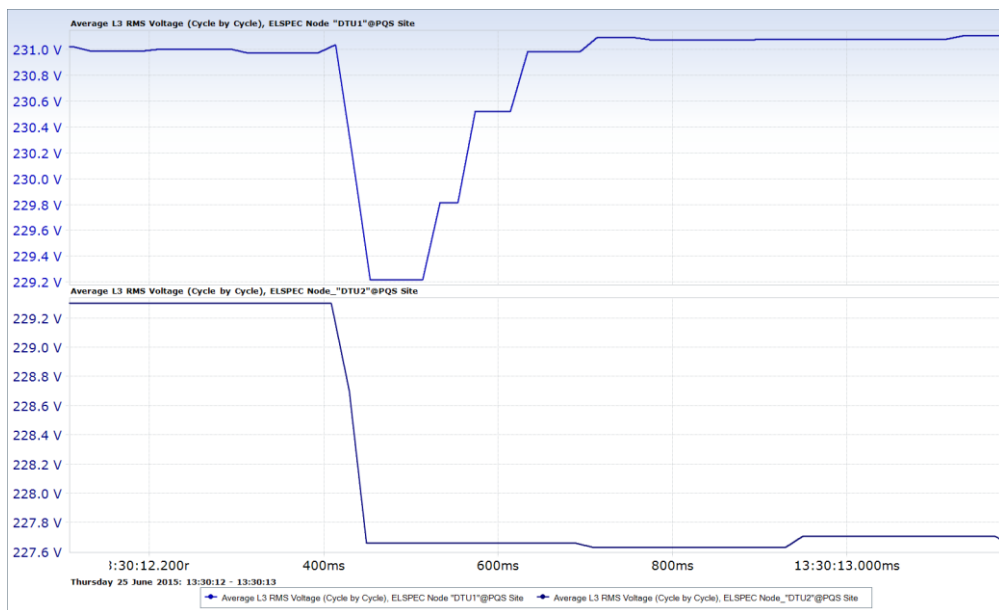
Fig. 32. Zoom-in of the phase-neutral voltage on phase c

Fig. 32 outcome:

$\Delta V_{step\_}1 = 0.60$ V

$\Delta V_{step\_}2 = 0.71$ V

$\Delta V_{step\_}3 = 0.46$ V

$\Delta Vprim = 0.00$ V

Results Analysis and Interpretation

From the zoom-in of the trends of the RMS values of the phase-neutral voltages at phase a at the two sides of the VOU, it can be noticed that, considering the time shift of 5 ms between the two measurement units, the drop at the primary side takes place during the first OLTC step: this could justify the fact that ΔV_{step_1} is smaller than ΔV_{step_2}. On the other hand, from the zoom-in of the phase-neutral voltages at phase c, it is noticeable that $\Delta V_{step\_1} \neq \Delta V_{step\_2} \neq \Delta V_{step\_3}$ even though the supply voltage is constant. This fact, which has been found in several more cases here not presented, indicates that there is not any correlation between the supply voltage and the size of ΔV_{step}.

Since, as demonstrated, the inconstancy of ΔV_{step} is not strictly due to a variation of the supply voltage, it has been decided to consider the behavior of whole tap activity that take place because of a voltage drop. In this sense the reference OLTC operation trend could be easily simplified as shown in Fig. 33.
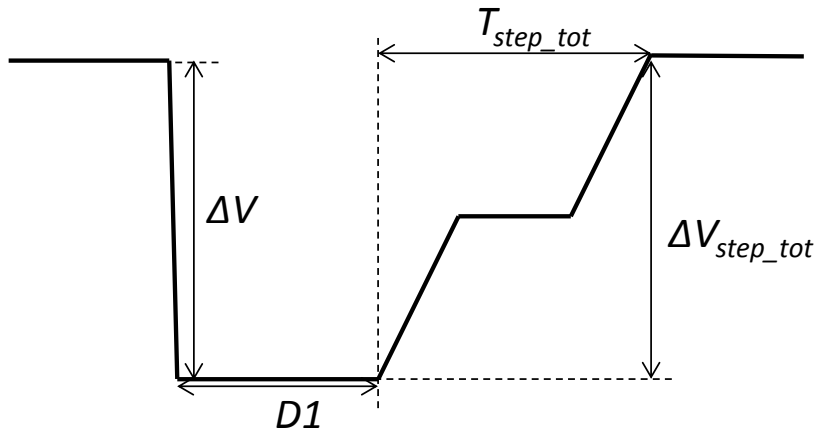
Fig. 33. Semplified reference OLTC tap operation

Thus, with reference to Fig. 33, henceforth the two main parameters that will be taken into account are the total voltage variation ΔV_{step_tot} and the time needed for the whole operation T_{step_tot}; while *D1* and ΔV mantein the same meaning previously defined.

An important operative parameter that it has been decided to calculate and monitor is the correction speed *CS*, which is calculated as:

$$CS = \frac{\Delta V step\_tot}{T_{step\_tot}} \quad \left[\frac{V}{s}\right] \tag{10}$$

The correction speed has been calculated independently for the three single-phase OLTCs, considering the mean values of the single operations that took place during both the sets of preliminary test performed. The three speeds amounted to:

$CS_a \approx 19\ V/s \approx CS_b \approx CS_c \approx 19\ V/s$

Another interpretation of the results is proposed.

Fig. 34 shows in detail the outline of the toroidal unit where the tap selector is placed, consisting in total of about 400 turns. The afore-reported results have also shown that every real tap activity is on average composed by 2 steps ΔV_{step} and that the tap selector concatenates about ±12 turns. Therefore it has been possible to conclude that the voltage difference caused by a single turn is very limited, justifying an inconstancy of the measured ΔV_{step} and delay-times. In fact, test results have shown that both ΔV_{step} and $D1$ are not constant.
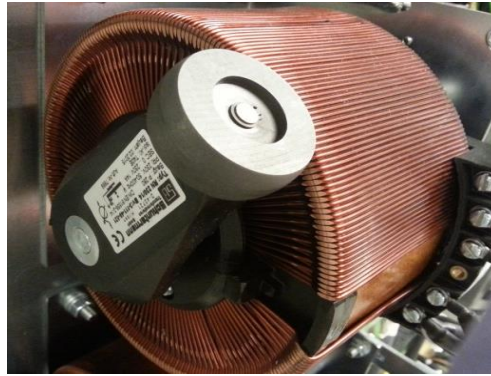
Fig. 34. Single-phase toroidal transformer and tap selector

As outcome of this operation analysis, it can be concluded that the actual tap actions described by 2 small steps ΔV_{step} could actually be considered as one. Therefore, the behavior of a single larger tap activity can be considered: the reference OLTC operation trend could then be easily simplified as the one reported in Fig. 33.
Specifically, as the average value of all the measured ΔV_{step} amounted to 0.72 V, it has been decided to consider values of 1.44 V for ΔV_{step_tot}. Consequently, a total number of steps of 32 (±16 from the '0-position') has been obtained, achieving in this way the expected regulation range ±10 % of the rated voltage. Regarding T_{step_tot} and $D1$, the value of 60 ms has been chosen based on the considerations made on the test results.

The outcome of this very last analysis has been considered as reference for the modeling of the transformer's real tap behavior in DIgSILENT PowerFactory simulation environment, as will be presented in Section 4.4.

4 CHARACTERIZATION OF THE VOU AND MODELING

For a complete investigation of the transformer, in addition to the tap activity operation, also some structural internal parameters needed to be calculated. In this regards, the open-circuit test and the short circuit test are the standard procedure for a complete and exhaustive characterization of a power transformer.

Both the open-circuit and the short-circuit test are based on the reference approximate equivalent circuit referred to the primary side (Fig. 35), which allows to represent in a simple way the inner behavior of the transformer itself.
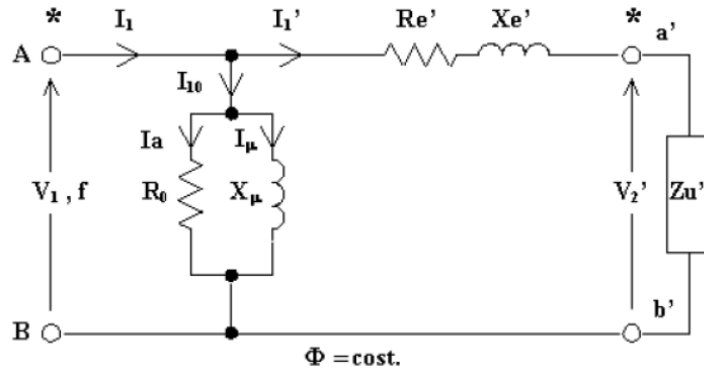
Fig. 35. Approximate equivalent circuit referred to the primary side

The equations and the definitions where the circuit diagram is based on are:

- Secondary side current referred to the primary side: $\bar{I}'_1 = -\frac{1}{n}\bar{I}_2$ (11)
- Primary side current: $\bar{I}_1 = \bar{I}'_1 + \bar{I}_0$ (12)
- Off-load current: $\bar{I}_0 = \bar{I}_a + \bar{I}_\mu$ (13)
- Primary side voltage: $\bar{V}_1 = \bar{Z}'_e\bar{I}'_1 + \bar{V}'_2$ (14)
- Secondary side voltage referred to the primary side: $\bar{V}'_2 = -n\bar{V}_2$ (15)
- Load impedance referred to the primary side: $\bar{Z}'_u = n^2\bar{Z}_u$ (16)
- Impedance: windings resistance + leakage reactance:
$$\bar{Z}'_e = R'_e + jX'_e = R_1 + n^2R_2 + j(X_1 + n^2X_2) \qquad (17)$$
- Off-load Impedance: $\bar{Z}'_0 = \frac{R_0 \cdot jX_0}{R_0 + jX_0}$ (18)

4.1 Open Circuit Test

The 'Open circuit test' or 'no-load test' on a three-phase transformer is performed to determine 'no-load loss (core/iron loss)' and 'no load current I_0'.
The circuit diagram for open circuit test is shown in Fig. 36.
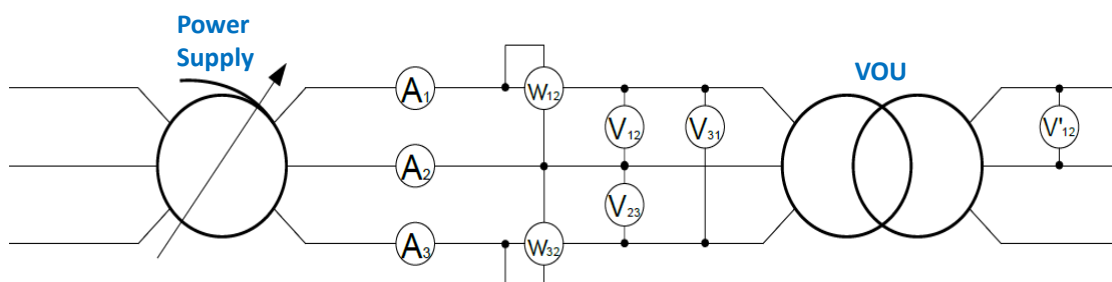
Fig. 36. Circuit diagram for open circuit test

As it can be deduced from the circuit diagram, the needed measurement instruments are:

-         3 ammeters (at the primary side);
-         3 voltmeters (at the primary side);
-         2 wattmeters (at the primary side);
-         1 voltmeter (at the secondary side).

In order to perform this test two ELSPEC units connected at the two sides of the VOU have been used.
The open circuit test has been repeated for all the possible tap positions (all the transformation ratios), in order to find out their dependency to no-load current and iron loss.
The ammeter reading gives the no load current I_0. Since the secondary side is open, there is no current flowing at the secondary side, and so there is no output power. Hence, the input power only consists of core losses and copper losses, which can be neglected, since almost the whole current flows through the 'off-load branch'. The input power is so considerable equal to the core losses (P_0), measured at the primary side.
The voltage measurement at the secondary side enables to find the voltage transformation ratio (n), used as reference for the trend of I_0 and P_0.

With reference to the figure above, the equations which the test is based on are:

$$n = \frac{V_{12}}{V'_{12}}$$ (19)

$$P_0 = W_{12} + W_{32} \tag{20}$$

$$P_0 = \sqrt{3}V_n I_0 \cos\varphi_0 \rightarrow \varphi_0 = \cos^{-1}\left(\frac{P_0}{\sqrt{3}V_n I_0}\right) \tag{21}$$

$$i_{0\%} = \frac{I_0}{I_n} \cdot 100\% \tag{22}$$

$$|\bar{Z}_0| = \frac{V_n}{\sqrt{3}\,I_0} \tag{23}$$

$$\rightarrow \qquad R_0 = \frac{|\bar{Z}_0|}{\cos\varphi_0} \tag{24}$$

$$\rightarrow \qquad X_\mu = \frac{|\bar{Z}_0|}{\sin\varphi_0} \tag{25}$$

4.1.1 Numerical and Graphical Results

The test has been performed twice: on the 1st ('Test1') and on the 10th of July ('Test2'). Graphical and numerical results in terms of iron losses, off-load current, off-load impedance and cosphi0 are reported in Fig. 37-40 and Tables 4 and 5, respectively.
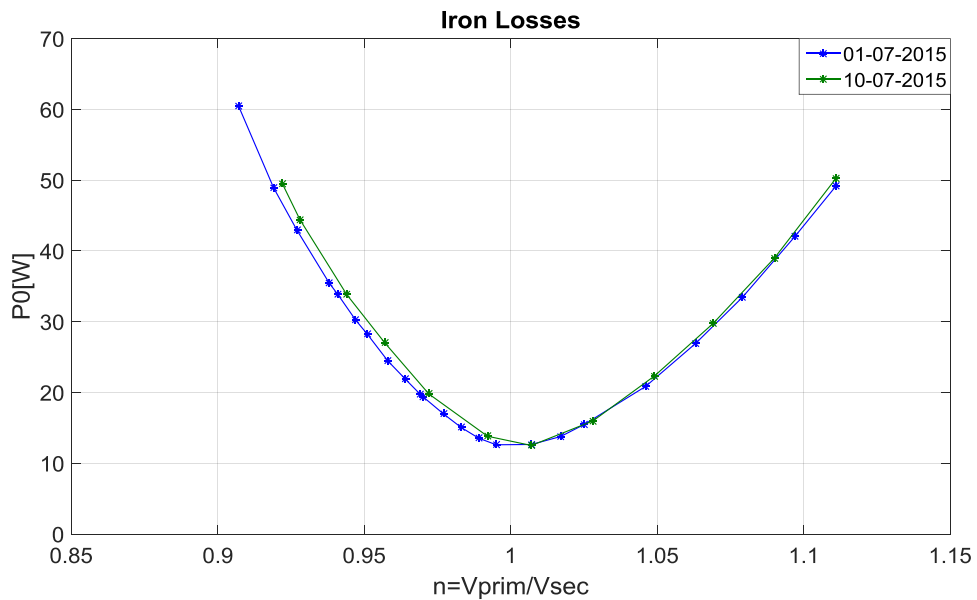
Fig. 37. Iron losses for for different n
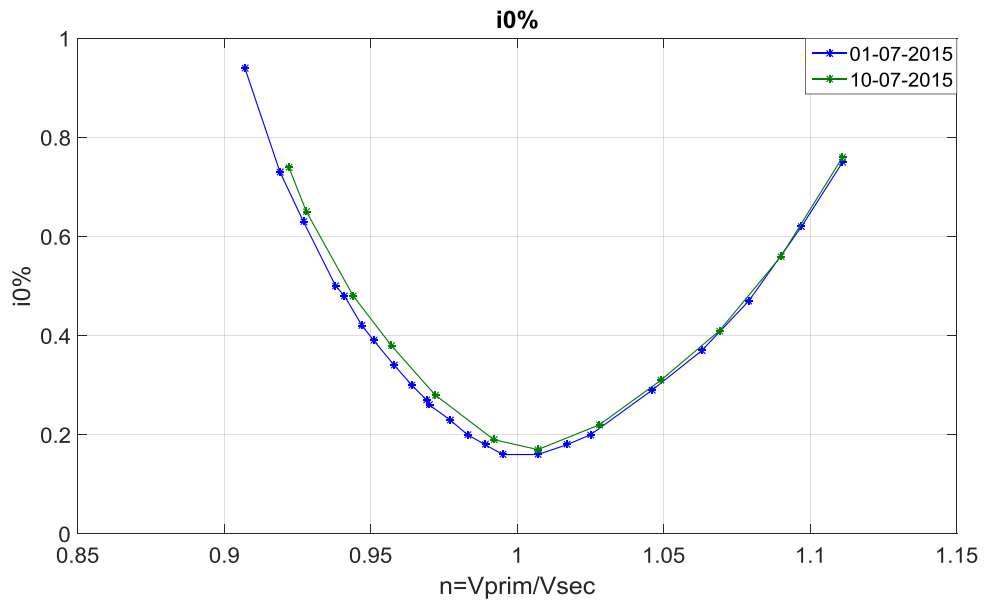
Fig. 38. Off-load current for for different n
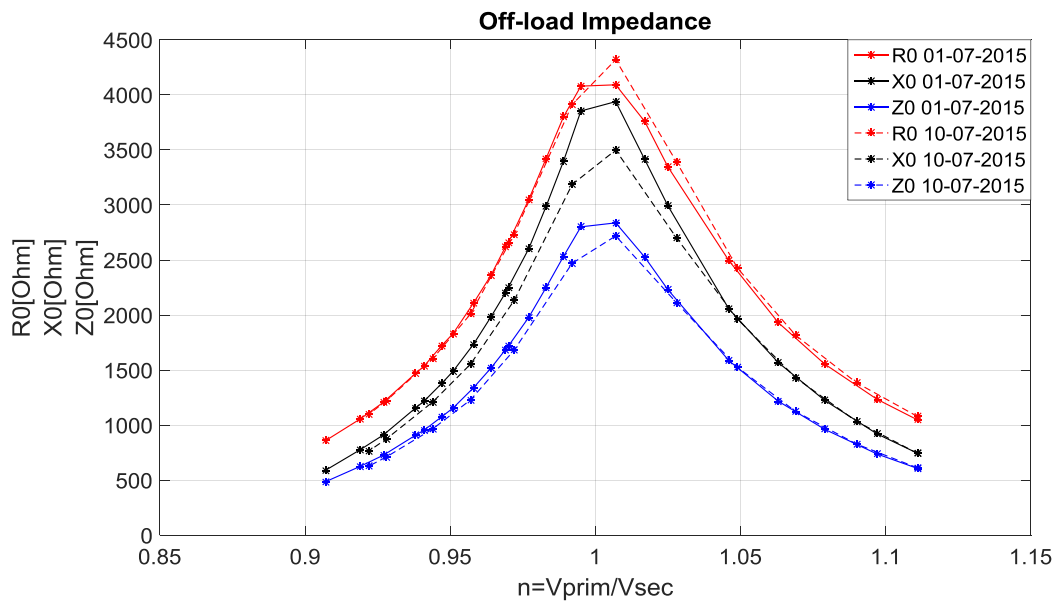
Fig. 39. Off-load impedance for for different n
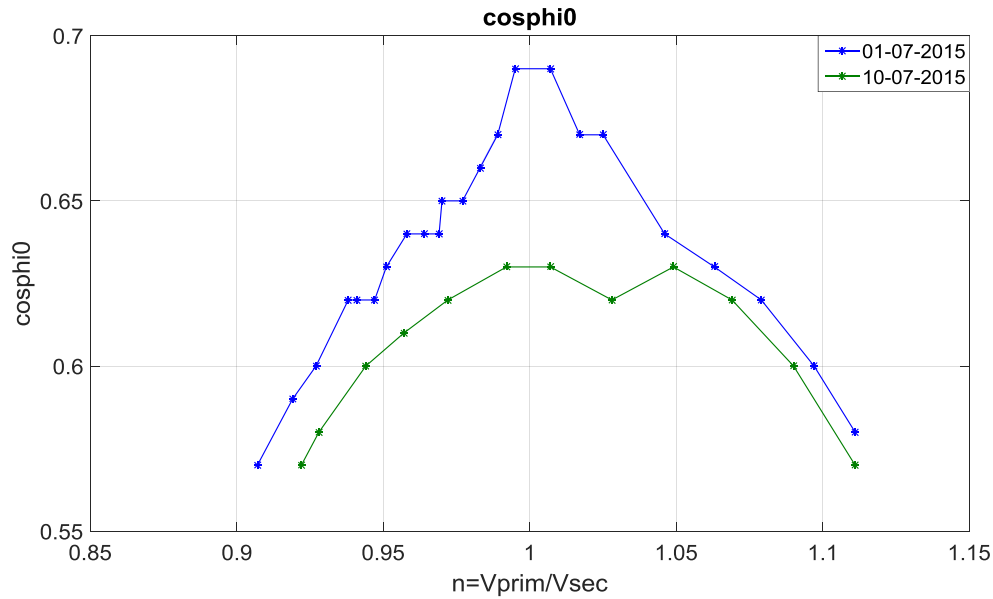
Fig. 40. Iron losses for for different n

Table 4. Numerical Results Test 1 (01-07-2015)

n=Vprim/Vsec	i0%	Z0 [Ω]	cosϕ0	R0 [Ω]	X0 [Ω]	P0 [W]
0.907	0.94%	486.18	0.57	858.79	589.79	60.52
0.919	0.73%	626.22	0.59	1056.75	777.43	48.93
0.927	0.63%	728.01	0.60	1208.83	911.94	42.92
0.938	0.50%	908.24	0.62	1469.65	1155.25	35.46
0.941	0.48%	955.16	0.62	1537.05	1219.14	33.82
0.947	0.42%	1075.48	0.62	1721.70	1377.24	30.24
0.951	0.39%	1156.55	0.63	1832.67	1490.92	28.24
0.958	0.34%	1339.58	0.64	2108.98	1734.40	24.47
0.964	0.30%	1518.10	0.64	2359.92	1982.82	21.88
0.969	0.27%	1685.32	0.64	2619.48	2201.44	19.78
0.970	0.26%	1718.04	0.65	2657.09	2252.16	19.41
0.977	0.23%	1978.00	0.65	3046.67	2600.62	16.98
0.983	0.20%	2249.43	0.66	3420.81	2985.75	15.08
0.989	0.18%	2532.30	0.67	3799.89	3396.42	13.56
0.995	0.16%	2801.28	0.69	4079.19	3853.64	12.62
1.007	0.16%	2837.38	0.69	4091.18	3938.50	12.66
1.017	0.18%	2526.28	0.67	3757.71	3412.58	13.79
1.025	0.20%	2229.89	0.67	3345.34	2991.35	15.49
1.046	0.29%	1586.03	0.64	2494.35	2054.94	20.87
1.063	0.37%	1217.83	0.63	1932.01	1568.74	26.92
1.079	0.47%	962.41	0.62	1554.83	1225.37	33.44
1.097	0.62%	738.64	0.60	1235.70	921.35	42.08
1.111	0.75%	606.86	0.58	1047.75	744.44	49.20

Table 5. Numerical Results Test 2 (10-07-2015)

n=Vprim/Vsec	i0%	Z0 [Ω]	cosφ0	R0 [Ω]	X0 [Ω]	P0 [W]
1.111	0.76%	612.02	0.57	1078.60	743.25	50.28
1.090	0.56%	828.07	0.60	1384.84	1033.11	39.02
1.069	0.41%	1123.62	0.62	1816.09	1430.22	29.75
1.049	0.31%	1525.28	0.63	2424.72	1962.12	22.34
1.028	0.22%	2110.74	0.62	3388.25	2698.28	15.99
1.007	0.17%	2718.50	0.63	4319.01	3498.45	12.52
0.992	0.19%	2470.53	0.63	3912.32	3186.16	13.83
0.972	0.28%	1681.29	0.62	2733.39	2132.39	19.80
0.957	0.38%	1229.88	0.61	2010.08	1554.91	27.00
0.944	0.48%	967.04	0.60	1605.12	1211.61	33.82
0.928	0.65%	711.56	0.58	1222.20	875.18	44.42
0.922	0.74%	628.66	0.57	1099.91	766.14	49.50

4.1.2 Conclusions

From the plots above it is possible to notice the symmetric trend of both the iron loss and the no-load current with respect to the unitary turn ratio.

The minimum values are respectively around 12.6 W and 0.16% (the off-load current is presented in percent with reference to the rated value, i.e. 50 A), and take place for n=1. The extreme turn ratio cases are characterized by iron losses of 50 W and off-load current of 0.75%.

4.2 Short-Circuit Test

Although the standard procedure for the characterization of a power transformer includes the short-circuit test, in this study its performance has not been possible due to the lack of availability of an autotransformer able to provide the appropriate short-circuit voltage, i.e., the reduced supply voltage needed for such a test. Therefore, it has been decided to calculate the copper losses P_{Cu} through an indirect procedure, through the calculation of the operative losses that take place during normal on-load operations.

With reference to equation (26), the copper losses P_{Cu} are calculated as difference of the calculated load-losses under nominal load condition P_{loss_n} P_{loss_load} and the iron losses P_0, divided by the square of the grade of loading $(I_{load}/I_n)^2$, which takes into account the square dependency to the loading level.:

$$P_{Cu}=(P_{loss\_n}-P_0)/(I_{load}/I_n)^2=P_{loss\_n}-P_0 \qquad (26)$$

Practically, in the performed tests nominal conditions have been utilized, so that the factor $(I_{load}/I_n)^2$ has been considered equal to 1

4.3 On-Load Test

This section presents the 'On-Load Test', i.e. the investigation of the behavior of the transformer under a specific balanced load condition.
The aim of the test is the determination of the operative inner losses of the transformer for different turn ratio, set manually by adjusting the output reference voltage.
It has been decided to connect the load directly to the secondary side of the transformer, without the cable in between.
The test has provided the operative inner losses of the transformer, as difference between the input and the output measured active powers.

The load has been set firstly at 10 kW for Test 1, while the repetition (Test 2) has been characterized by a lower loading: 9 kW.
This change has been acted since the load behaves as a 'fixed-impedance' load: the set power (P_{set}) is actually absorbed whether the supply voltage (V_{supply}) is equal to the rated value of 230 V (V_{nom}). Whenever the supply voltage is different from the nominal one, the absorbed power ($P_{absorbed}$) changes accordingly, following a square dependency, as described by the following equation:

$$P_{absorbed} = P_{set} \left(\frac{V_{supply}}{V_{nom}}\right)^2 \qquad (27)$$

Because of this, for the Test 1 it has been decided to consider only turn ratio > 1, i.e. conditions characterized by voltage at the secondary side lower of the one at the primary side, so that the actual active power absorbed by the load could not exceed the set one.
As for the Test 2 the set load power has been reduced, it has been possible to perform the test considering different output reference voltages within the whole regulation range ± 10% of the rated value.

4.3.1 Numerical and Graphical Result

The test has been performed twice: on the 1st ('Test1') and on the 13th of July ('Test2'). Graphical results of the measured on-load losses are reported in Fig. 41, while results in terms of voltage, current and power at the two sides and total losses as well are presented in Tables 6 and 7, respectively for the two tests.
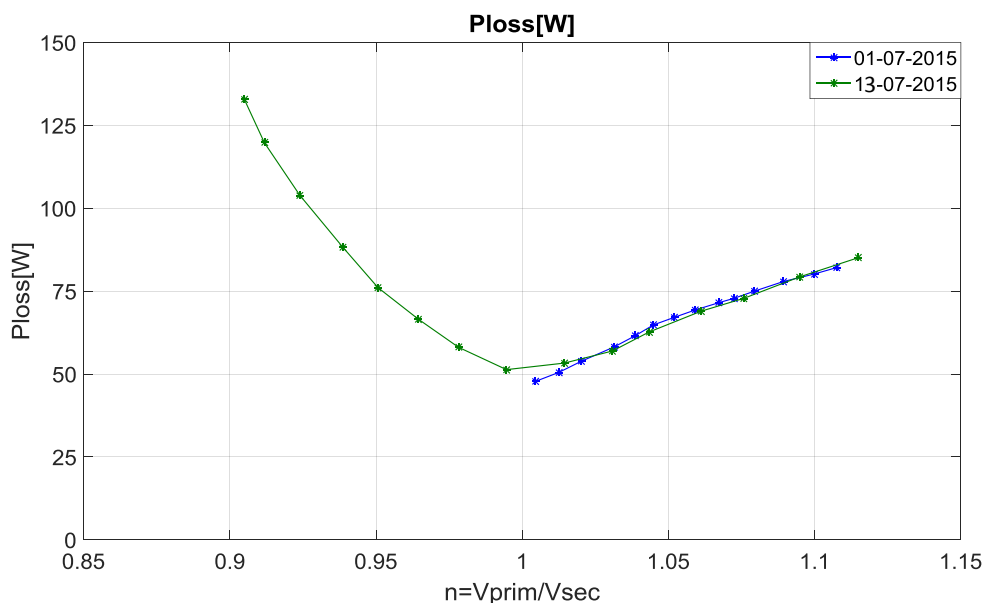
Fig. 41. On-load losses for for different n

Table 6. Numerical Results Test 1 (01-07-2015)

$n=V_{prim}/V_{sec}$	V_{prim} [V]	Ia_{prim} [A]	Pa_prim [W]	V_{sec} [V]	Ia_sec [A]	Pa_sec [W]	P_{loss} [W]
1.11	226.44	37.89	8580.11	204.45	41.58	8497.97	82.14
1.10	226.99	38.53	8744.85	206.40	41.99	8664.68	80.18
1.09	226.90	39.27	8910.88	208.30	42.42	8832.95	77.93
1.08	226.42	39.88	9029.97	209.76	42.70	8954.94	75.03
1.07	226.24	40.36	9129.72	210.96	42.94	9056.88	72.85
1.07	225.92	40.69	9190.91	211.71	43.09	9119.41	71.51
1.06	226.34	41.35	9358.44	213.72	43.48	9289.12	69.32
1.05	226.40	41.89	9483.26	215.21	43.77	9416.15	67.11
1.04	226.63	42.48	9626.18	216.90	44.09	9561.34	64.83
1.04	226.69	42.98	9742.19	218.28	44.36	9680.67	61.53
1.03	226.79	43.58	9880.94	219.89	44.68	9822.77	58.17
1.02	226.41	44.43	10058.56	221.96	45.09	10004.74	53.82
1.01	226.89	45.16	10242.91	224.08	45.50	10192.38	50.53
1.00	226.61	45.81	10377.85	225.61	45.80	10330.08	47.78

Table 7. Numerical Results Test 2 (13-07-2015)

n=V_{prim}/V_{sec}	V_{prim} [V]	Ia$_{prim}$ [A]	Pa_prim [W]	V_sec [V]	Ia_sec [A]	Pa_sec [W]	P$_{loss}$ [W]
1.11	229.13	32.45	7434.37	205.51	35.77	7349.27	-204.40
1.09	228.92	33.67	7707.37	209.09	36.49	7628.06	-208.00
1.08	228.92	34.87	7981.72	212.79	37.18	7908.86	-211.71
1.06	228.89	35.79	8191.35	215.70	37.66	8122.38	-214.63
1.04	229.07	36.99	8471.49	219.55	38.31	8408.80	-218.50
1.03	228.78	37.80	8646.61	221.94	38.71	8589.65	-220.91
1.01	228.62	38.97	8907.92	225.39	39.29	8854.60	-224.37
0.99	228.25	40.42	9225.09	229.49	39.98	9173.75	-228.49
0.98	227.99	41.74	9515.40	233.07	40.59	9457.33	-232.10
0.96	228.13	42.97	9801.49	236.53	41.17	9734.93	-235.57
0.95	228.20	44.25	10096.21	240.05	41.75	10020.13	-239.10
0.94	228.15	45.38	10352.82	243.06	42.24	10264.61	-242.12
0.92	227.97	46.80	10668.60	246.73	42.83	10564.71	-245.81
0.91	227.84	48.03	10943.41	249.88	43.33	10823.64	-248.96

4.3.2 Conclusions

From the results of Test 2, it is possible to notice that the trend of the inner losses presents a minimum point for n = 1, while when n ≠ 1 the losses increase, although not perfectly symmetrically.

As already said, for the Test 1 only voltages at the secondary side lower than the one at the primary side have been considered, i.e. turn ratio n > 1. Nevertheless the obtained results are the same, so it is possible to conclude that also for n < 1 the trend could have been the same that has been found with the Test 2.

As further conclusion, it can be said that the two tests have provided the same results in terms of inner power losses, even though the set load power were different.

As overall result, as difference of the iron losses to the load-losses for the different turn ratios, the copper losses are so characterized: the extreme positions are both characterized by P_{Cu} of 85 W, while of 35 W at the central position, i.e., 0.73 % and 0.3 % of the rated single-phase unit power, respectively.

Finally it deserves to be noted that, in order to complete the characterization of the transformer (i.e. in order to determinate the short-circuit voltage V_k, i.e., the reduced supply voltage needed for such a test, which makes the nominal current flowing at the secondary side), the Short-Circuit test needs to be performed.

It has therefore been set arbitrarily to 4 % of the rated voltage, according to the realistic value utilized in the previously mentioned simulation works [8]–[10].

4.4 OLTC Modeling

All the elements involved in the practical tests have been modeled in DIgSILENT PowerFactory software environment, with the aim of reproducing as realistically as possible their operational behavior during the experiments. In the following sections the modeling of the VOU is presented.

In order to perform independent single-phase changes of the transformation ratios in the simulation tool, the real OLTC Dyn transformer has been modeled with three single-phase units independently controlled, whose secondary sides are connected between an earthed neutral point and a different phase of the modeled experimental LV grid. Each single-phase transformer has been set with rated power P_n of 11.66 kVA and characterized by a regulation capability of ±10 % of the nominal voltage at the secondary side.
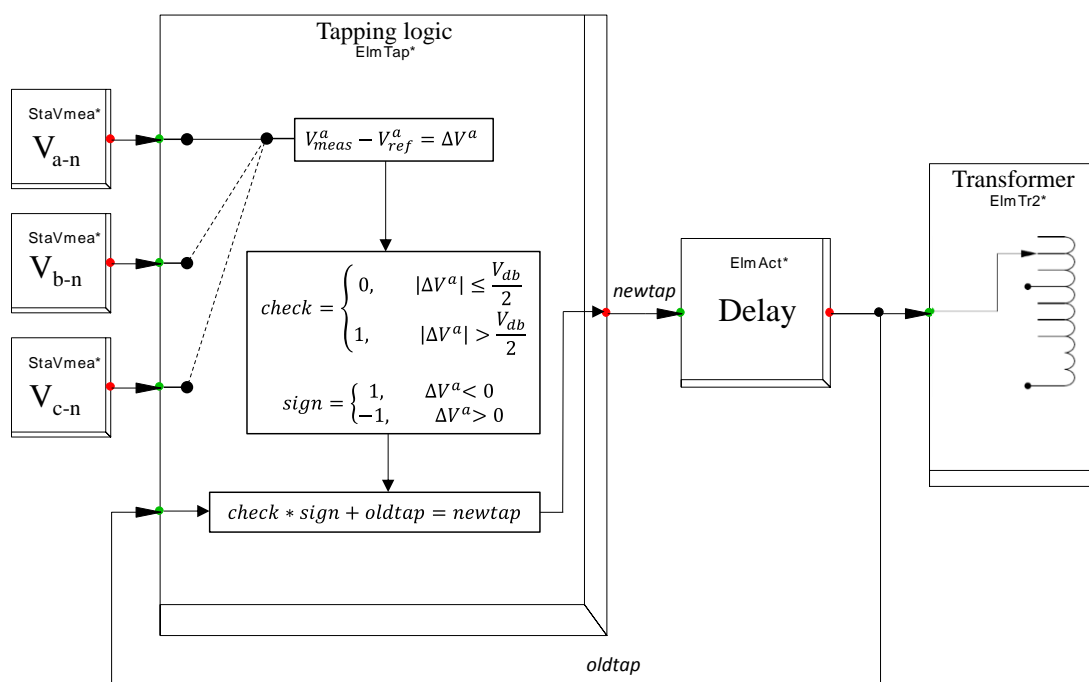
Fig. 42. Control scheme for the decoupled-phase OLTC transformer

With the aim of representing the investigated tap activity reported in Fig. 33, two blocks have been built to model the control scheme, shown in Fig. 42. The first one calculates the deviation ΔV of the measured local voltage V_{meas} from the reference voltage V_{ref}, which is manually set as input value. According to size and sign of ΔV, two appropriate internal parameters *check* and *sign* assume respectively values of 0/+1 or -1/+1. They aim both at activating the tap action – whenever the deviation exceeds half of the allowed dead band set at 1 % of the rated voltage – and at deciding whether the turns ratio needs to be increased or decreased. If the calculated new tap position *newtap* overcomes

the allowed extreme tap positions (±16), then ±16 is provided as output. The output of the first block is so delayed by 120 ms by the second block, a simple delay-block which includes both the intentional delay-time *D1* and the operational time T_{step_tot} described in Paragraph 3.2, in order to guarantee the total effective time needed by the transformer for a physical tap operation. The obtained delayed tap position is both applied to the transformer unit and utilized as retro-input for the next simulation step. The 3 tap-changing devices operate independently, referring each one to the respective single-phase voltage measurement.

For a complete and realistic representation of the transformer, iron losses, no-load current and copper losses have been set according to the results presented in Paragraph 3.2. Another required internal parameter is the short-circuit voltage V_k, which, as explained above, could not be calculated. It has therefore been set arbitrarily to 4 % of the rated voltage, according to the realistic value utilized in the previously mentioned simulation works [8]–[10]

5 VOU MODEL VALIDATION

The experimental activity presented in this section focuses on the analysis of the effectiveness of the VOU operations under conditions characterized by different power flow directions on the three phases, considering two operative scenarios.

This section focuses on the evaluation of the real tap-changers activities and the implemented models. With the purpose of evaluating the modeled system, the results obtained from the practical tests are compared to the simulations' ones, by monitoring and calculating the same parameters and indexes.

5.1 Scenarios definition

With the purpose of monitoring the dynamics of the tap actions taking place as the consequence of a single-phase load changing, a preliminary test has been performed. In this regard, Scenario #0 has been defined – see Table 8. It foresees the biggest possible single-phase (phase *c*) load increment occurring with a single event, i.e., a step from 0 kW to a loading condition of 11.6 kW. The other two phases' power flows remain unchanged. Phase *a* is affected by reverse power flow coming from the constant current injection of 16 A (corresponding to 3.4 kW) from the EV, while phase *b* is constantly loaded at 11.6 kW. This particular unbalanced condition has been chosen because it is relevant to analyze the single-phase tap action whenever the system is heavily stressed by reverse power flow and maximum loading condition.

Table 8. Scenario #0

	Phase a [kW]	Phase b [kW]	Phase c [kW]
Starting condition	-3.4 (-16 A)	11.6	0
Ending condition	-3.4 (-16 A)	11.6	11.6

Two more operative scenarios aim at verifying the decoupled-phase OLTC effectiveness under conditions characterized both by balanced/unbalanced conditions and different power flow directions on the three phases, while considering events on loads' power and EV's current injection. Specifically, Scenario #1 is mainly based on the consideration of balanced increases of power absorptions evenly by the three single-phase loads, by reason of 1 kW-steps from 0 kW to 11 kW every 3 minutes. The objective of Scenario #1 is the verification of appropriate operability of the three independent tap changers, in the case of balanced loads conditions, i.e., under a conventional power flow situation. In Table 9, the operation procedure and the actual single-phase set active power are reported.

Table 9. Scenario #1

Time of operation	Phase a [kW]	Phase b [kW]	Phase c [kW]
T=0s	0	0	0
T=28s	1.1	1.1	1.1
T=224s	2.2	2.2	2.2
T=390s	3.4	3.4	3.4
T=565s	3.7	3.7	3.7
T=751s	4.5	4.5	4.5
T=930s	5.6	5.6	5.6
T=1154s	6.7	6.7	6.7
T=1304s	7.8	7.8	7.8
T=1472s	9.3	9.3	9.3
T=1650s	10.8	10.8	10.8
T=1828s	11.6	11.6	11.6

For the second investigated operative scenario, the load on phase a has been replaced by the EV, while resistive single-phase loads have been maintained connected to phases b and c. Scenario #2 is thus characterized by increasing power injected by the EV, considering constant active power absorption (6.7 kW) on the other two phases. As at any considered situation the three phases are affected by different power flows in terms of both direction and loading, it is clear that the main objective of Scenario #2 is the analysis of the operations of the decoupled-phase OLTC in presence of different unbalanced situations and power flow directions. As described in Section II-E, the VMS of the EV allows manual adjustment of the current. Considering this technical feature, the increase of the injected power at Scenario #2 has been obtained manually adjusting the current from 0 to 16 A with 2 A–steps every 3 minutes, reported in Table 10 in terms of active power.

Table 10. Scenario #2

Time of operation	Phase a [kW]	Phase b [kW]	Phase c [kW]
T=0s	-0.1 (-2 A)	0	0
T=48s	-0.1 (-2 A)	6.7	6.7
T=399s	-0.8 (-4 A)	6.7	6.7
T=560s	-1.3 (-6 A)	6.7	6.7
T=737s	-1.7 (-8 A)	6.7	6.7
T=915s	-2.1 (-10 A)	6.7	6.7
T=1097s	-2.6 (-12 A)	6.7	6.7
T=1277s	-3.0 (-14 A)	6.7	6.7
T=1457s	-3.4 (-16 A)	6.7	6.7

5.2   Results analysis

Graphical results are presented in terms of phase-neutral voltages both at the OLTC and the remote bus. For Scenario #2, in order to analyze the effects of unbalanced conditions, also the neutral-ground voltage at the remote bus has been monitored. Moreover, at either terminal of the cable, the voltage unbalance factor (VUF) has been calculated. equation (31) describes the VUF, defined as the ratio between the negative and the positive voltage components in percent [17].

$$VUF_\% = V_{neg\_seq}/V_{pos\_seq} \cdot 100 \tag{31}$$

5.2.1   Results – Scenario #0

T he results of Scenario #0 are reported in Fig. 43, where the tap operations from both the practical test and simulation activities are presented – named *V-c-Exp* and *V-c-Sim*, respectively. It can be noticed that in both cases the 11.6kW-step load increase causes a voltage drop of roughly 11 V (i.e., 0.048 p.u.) and the time necessary to rise the voltage up within the dead band amounts to approximately 1 s. The dynamics of the tap actions, investigated in Paragraph 3.2 and implemented in the simulation tool as described in Paragraph 4.4, reflect the expectations. This could lead to the conclusion that the implemented model could represent properly and realistically the real behavior of the analyzed OLTC transformer.
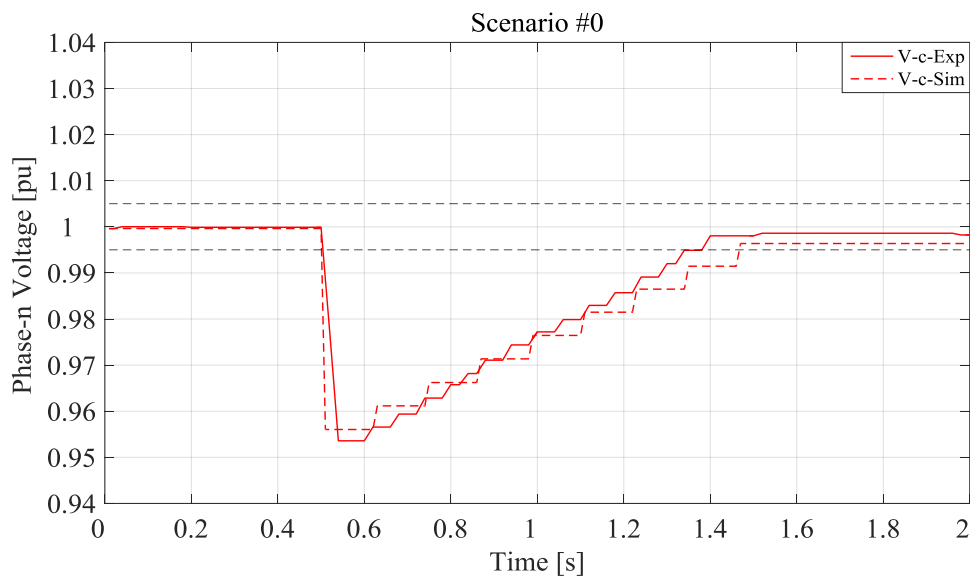

Fig. 43. Tap actions for phase c for Scenario #0

5.2.2 Results – Scenario #1

For each phase, the reference voltage V_{ref} (reported in Table 11) has been set in accordance with the voltage supplying the primary side, permitting to start the study with the tap selector at the '0-position' (unitary turns ratio). In order to compare efficiently the results, each phase-neutral voltage has been plotted in per unit, according to the respective V_{ref}.

Table 11. Voltage references for Scenario #1

V_{ref_a} [V]	V_{ref_b} [V]	V_{ref_c} [V]
233.6	233.9	234.4

Fig. 44 and Fig. 45 show the three phase-neutral voltages at the secondary side of the transformer and at the remote bus of the line, respectively. Comparisons of the results from the experimental test as well as the simulation study show that the modeled grid and components allow a realistic representation of the tested activities. In particular, from Fig. 44, it is possible to notice that, whenever one of the three phase-neutral voltages exceeds the lower allowed limit, a phase-independent tap action is performed. Fig. 45 shows that, since the OLTC controllers act based on local voltage measurements, voltages at the ending terminal bus are not considered in the control logic, being therefore characterized by increasing deviations from the nominal value, in accordance with the loads entity.

Fig. 44. Phase-neutral voltages at the OLTC bus for Scenario #1

Fig. 45. Phase-neutral voltages at the remote bus for Scenario #1

5.2.3   Results – Scenario #2

For Scenario #2, V_{ref} have been manually set as reported in Table 12. Again, each phase-neutral voltage has been plotted in per unit, according to the respective V_{ref}.

Table 12. Voltage references for Scenario #2

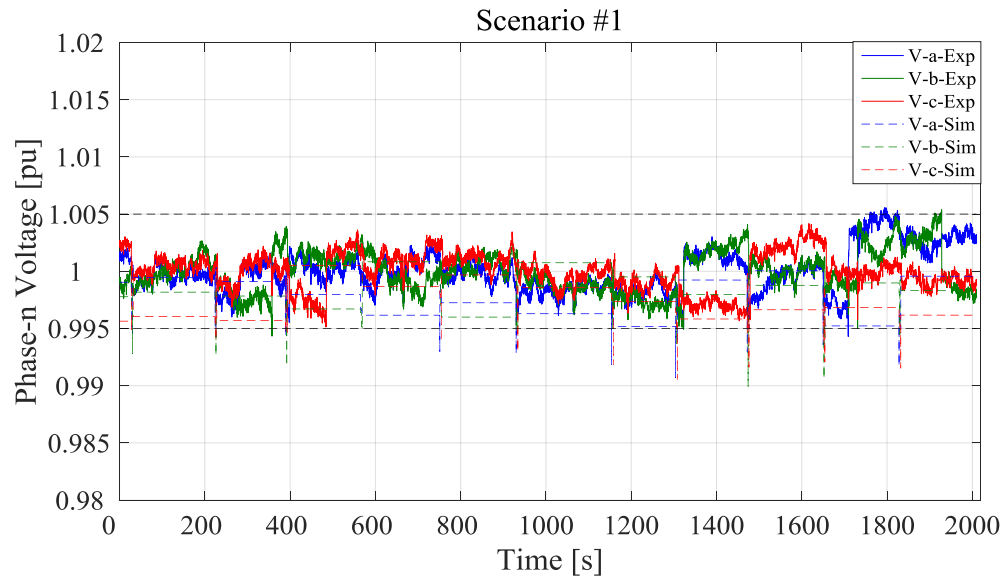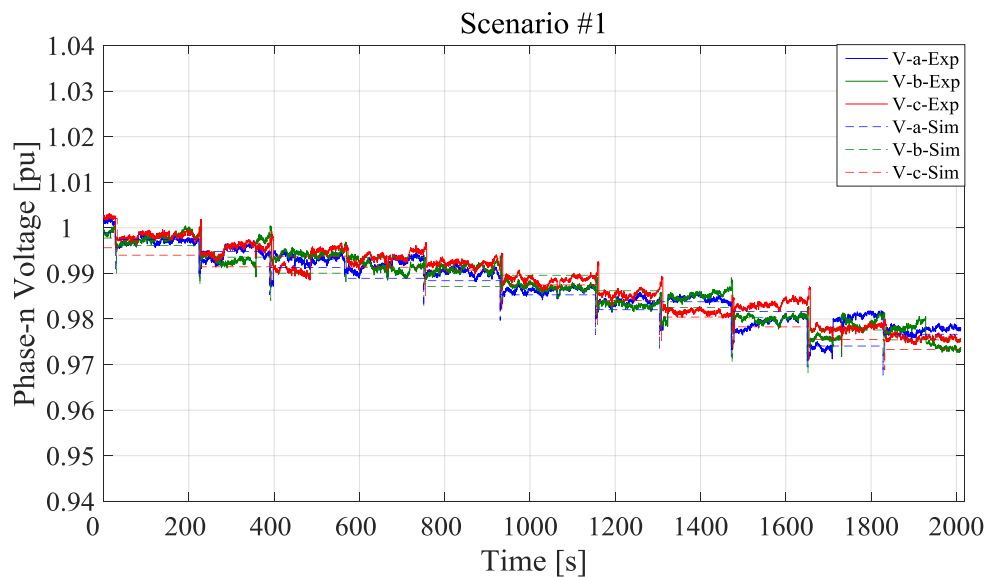| V_{ref_a} [V]	V_{ref_b} [V]	V_{ref_c} [V]
230.7	230.5	230.1
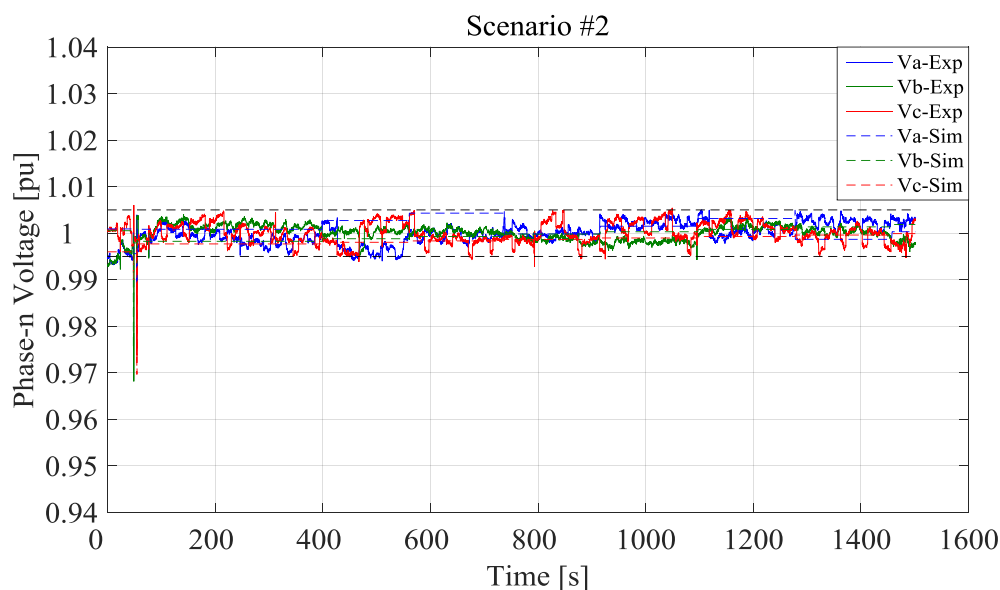
Fig. 46. Phase-neutral voltages at the OLTC bus for Scenario #2
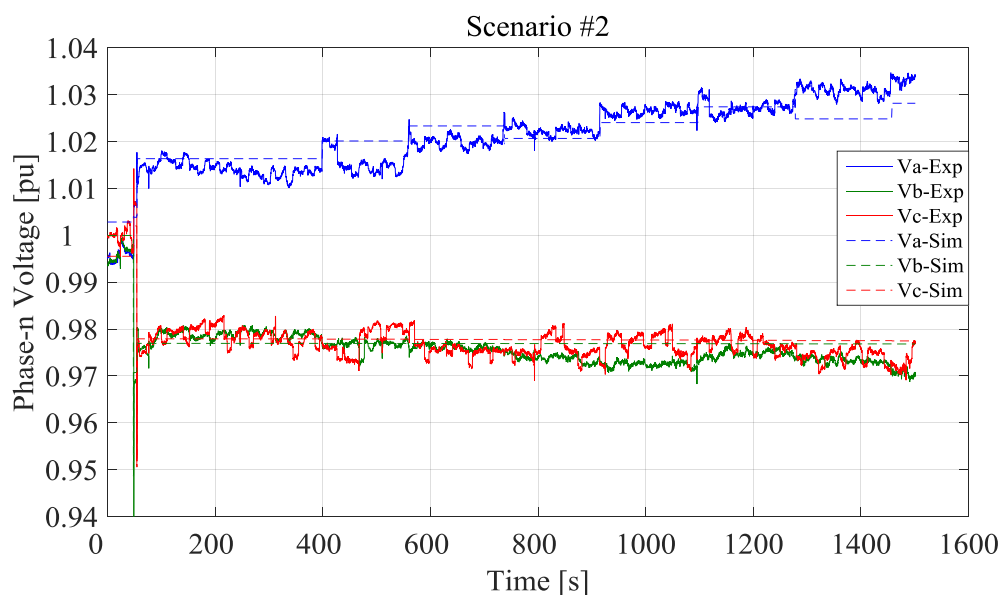
Fig. 47. Phase-neutral voltages at the remote bus for Scenario #2

Fig. 46 and Fig. 47 show the phase-neutral voltages at the two monitored points. In particular, from Fig. 46 it is possible to notice that, due to a relevant load-step of 6.7 kW after 28 s, the phase-neutral voltages on phases *b* and *c* exceed the lower allowed limit, leading to tap changing actions aiming at rising them within the dead band. Fig. 47 shows how voltages deviate differently on each phase at the remote bus: phase a pre-

sents an increasing voltage due to the increasing current injected by the EV, while phases b and c characterized by constant values after the cited initial reduction related to the load event.

From Table 13, it is noticeable that mean and maximum values of the neutral-ground voltage at the remote bus amount respectively to 1.92 % and 2.51 % of the rated voltage, both slightly higher than values obtained from the simulation. Regarding the VUF, its values at the remote bus are higher than those at the transformer level due to the higher voltage unbalance, making the negative sequence component more influent. It can also be noticed that values from the simulation at the OLTC bus are slightly higher than the real ones, while at the remote bus the results are very concordant in terms of mean values, below 2 %. Difference of almost 1 % has been found regarding the maximum value, which in the real test is even above 3%.

The not perfect match of experimental and simulation results, noticeable both from Table 13 and Fig. 47 (e.g., at t=~420 s, t=~1300 s), might be due to unavoidable continuous oscillations of the supply voltage at the primary side, which have not been possible to reproduce in the simulation study.

Table 13. Neutral-ground voltage and VUF for Scenario #2

Testing Activity	Neutral potential at remote bus		VUF at OLTC bus		VUF at remote bus	
	Mean Val.	Max Val.	Mean Val.	Max Val.	Mean Val.	Max Val.
Experimental	1.92%	2.51%	0.88%	1.54%	1.87%	3.16%
Simulation	1.66%	2.09%	1.42%	1.89%	1.85%	2.25%

6 INVESTIGATION OF DIFFERENT CONTROL LOGICS FOR THE VOU

In this section, we introduce four kinds of control logics (CL) related to phase-wise OLTC, namely:

- CL1, OLTC with local measurement.
- CL2, OLTC with remote measurement.
- CL3, line-drop compensation (LDC) control.
- CL4, modified LDC control.

The working principles of these four types of control logics are described as follows.

6.1 CL1: OLTC control with local measurement

Fig. 48 illustrates the operational principle of CL1. The OLTC will keep the local voltage constant within the range of the reference voltage. The reference voltage per phase is set manually with a screwdriver on the control unit. In an active distribution network, where distributed energy resources are connected, the voltages on the three phases can differentiate, meaning that the voltage at the remote busbar can violate the voltage band defined in the EN50160 standard, even though the voltage is regulated in a safe band at the secondary side of the OLTC transformer.
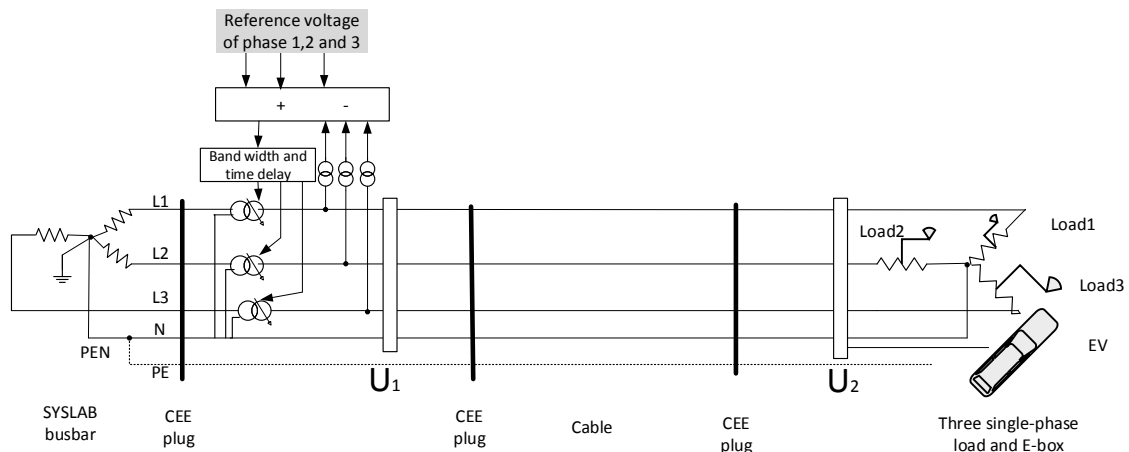

Fig. 48. Basic OLTC operational principle

6.2 CL2: OLTC with remote measurement

Fig. 49 shows the operational principle of the OLTC facilitated with remote measurement. It means that OLTC will keep the remote busbar voltage within the range. In contrast to CL1, the voltage profile at the secondary side of the OLTC transformer might be out of the voltage band when tapping, in order to regulate the voltage at the remote busbar.
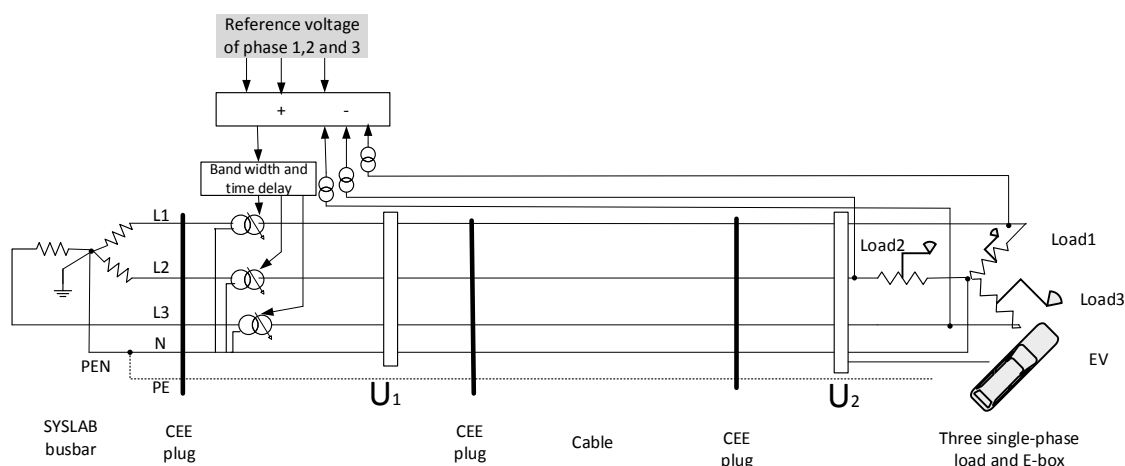

Fig. 49. Operational principle for an OLTC with remote measurement

6.3 CL3: LDC control

Compared to CL1 and CL2, the LDC control estimates the line-voltage drop based on the line-current measurement, resistance and reactance (R and X) and the local voltage measurement to get the voltage of the remote bus regulated within the range. The working principle is shown in Fig. 50. This is normally achieved by dial settings of the adjustable resistance and reactance elements of a unit, called the 'line-drop compensator', located on the control panel of the voltage regulator [15]. Determination of the appropriate dial settings depends upon whether or not any load or small renewable energy source unit is connected/disconnected to the feeder, between the voltage regulator and the regulation point. In terms of the details of selecting the proper R and X, this is described in [16]. Note that in an unbalanced network, the settings of R and X need to consider the mutual interactions among the three phases. Therefore, in addition to the phase current measurements, the neutral current and impedance also need to be measured.
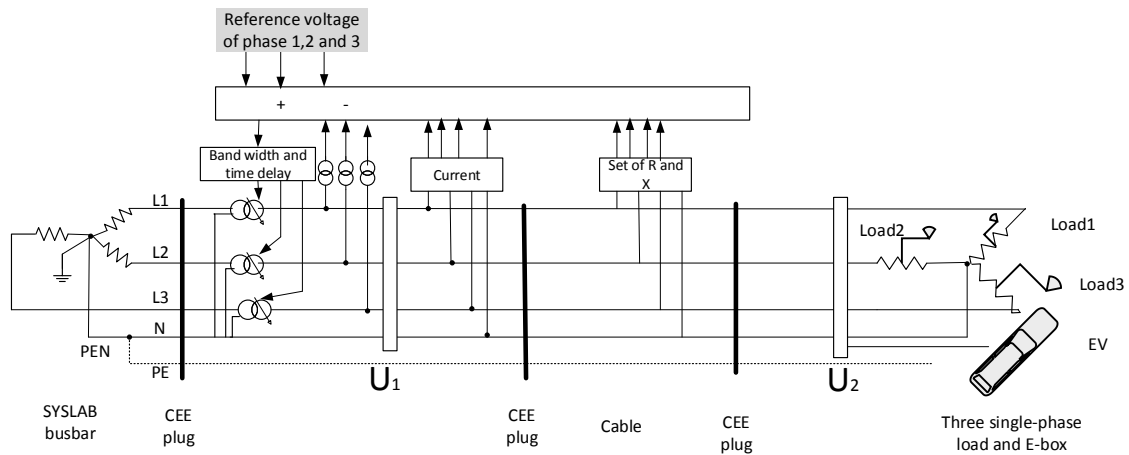
Fig. 50. Operational principle of LDC control

6.4 CL4: Modified LDC control

In this study, as the OLTC transformer does not have a control panel for setting *R* and *X* of the line, a modified LDC control logic is proposed. The proposal uses the manual voltage reference setting feature and regulates the voltage at the remote bus by considering the voltage drop. Three stages are included in the proposal which is represented in Fig. 51: 1) the voltage drop is calculated by measuring the local voltage, current and the known impedance value; 2) by knowing the voltage drop, we pre-set the position of the tap changer to counter the predicted voltage drop; and 3) the last stage of this proposal is a real-time operating control of the OLTC, which uses the same principle as the control logic CL1.

Fig. 51. Operational principle of modified LDC control

6.5 *Methodology of applying the LDC in an unbalanced distribution network*

In this section, we present two types of methods to calculate the voltage drop; namely, 'simple calculation' and 'complex calculation'. The simple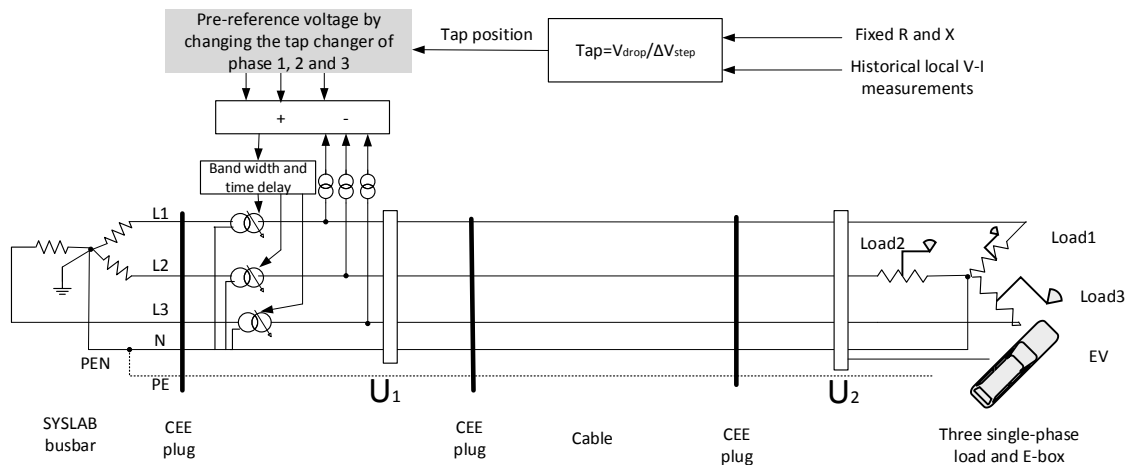 method approximates the voltage drop of an unbalanced distribution network to that of a balanced distribution network. The complex calculation considers the presence of the return wire. These two calculation methods are compared in the experimental work.

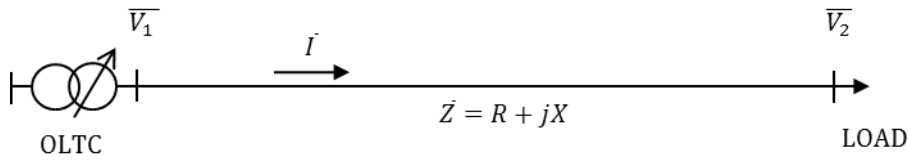### 6.5.1 *LDC voltage drop estimation using simple equation*

Fig. 52. Simple voltage drop estimation method

In a three-phase balanced distribution network represented in Fig. 52, the voltage drop along phase *a* can be estimated as:

$$\left|\overline{V_2}^a\right| = \left|\overline{V_1}^a\right| - \left(\left|\overline{Z_{aa}}\right| \cdot \left|\overline{I}^a\right|\right) \tag{28}$$

where $\left|\overline{V_1}^a\right|$ and $\left|\overline{V_2}^a\right|$ are the modules of the phase-neutral voltages at the starting and ending terminal of the line, respectively, $\left|\overline{I}^a\right|$ is the module of the current flowing on the considered phase, measured at the transformer level, while $\left|\overline{Z_{aa}}\right|$ is the module of the cable impedance. By knowing the impedance of the cable, as well as the measured voltage and current, the voltage at the remote bus can be calculated. Similarly, the voltage drops along the other two phases can be calculated.

6.5.2 *LDC voltage drop estimation using complex equation*

In an unbalanced power network, mutual interactions among the phases and between each phase and the neutral need to be taken into account for a correct grid analysis of the operation. Since the current on the neutral is no longer zero, a correspondent voltage drop along the neutral conductor appears, which cannot be neglected, as was the case for balanced situations. Therefore, considering the feeder as a single three-phase system composed of three phases and the neutral, the scheme reported in Fig. 53 needs to be considered.
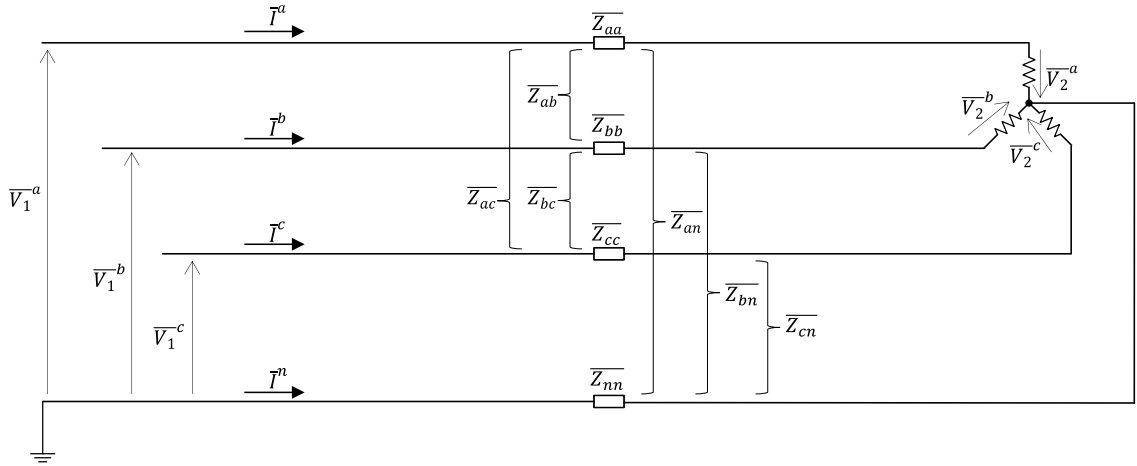
Fig. 53. Complex voltage drop estimation method

The single-phase voltage drop along the cable for phase *a* is calculated as in (29), by applying Kirchhoff's voltage law around the circuit, differently at each phase.

$$\overline{\Delta V}^a = \overline{V_1}^a - \overline{V_2}^a = (\overline{Z_{aa}} - \overline{Z_{an}}) \cdot \bar{I}^a + (\overline{Z_{ab}} - \overline{Z_{an}}) \cdot (\bar{I}^b + \bar{I}^c) + (\overline{Z_{an}} - \overline{Z_{nn}}) \cdot \bar{I}^n, \quad (29)$$

In our work, since the system is a LV system, $\overline{Z_{ab}}$ and $\overline{Z_{an}}$ can be neglected, so that equation (29) can be simplified as in equation (30).

$$\overline{\Delta V}^a = (\overline{Z_{aa}}) \cdot \bar{I}^a + (-\overline{Z_{nn}}) \cdot \bar{I}^n, \quad (30)$$

Similarly, the voltage drops along the other two phases can be calculated.

7 VOU COTROL LOGICS TESTING

In this section, we evaluate and compare three of the four control logics presented in Section 5. To compare their effects, the same loading and EV conditions are repeated while monitoring phase-neutral voltages at the two ending terminals of the cable.

7.1 Testing case description

To evaluate and compare the three control logics (CL1, CL2 and CL4) of the OLTC transformer in the experimental system (described in Section 5), phase-wise power profiles of the load and EV are described in Table 14. The setting of the power profiles considers the features of an unbalanced distribution network. The load on phase *a* has been changed to the power from the EV in Load/EV conditions 6 and 7, and the resistive single-phase loads of phases b and c have been maintained. As for any considered conditions, the three phases are affected by different power flows, in terms of both direction and loading, thus the main objective of this test is the analysis of the operations of the phase-wise OLTC in the presence of different unbalanced situations and power-flow directions. As the EV allows the manual adjustment of the current, the increase in the injected power at phase a has been set manually to 8 A and 16 A.

Table 14. Phase-wise power profiles of load and EV to compare three control logics

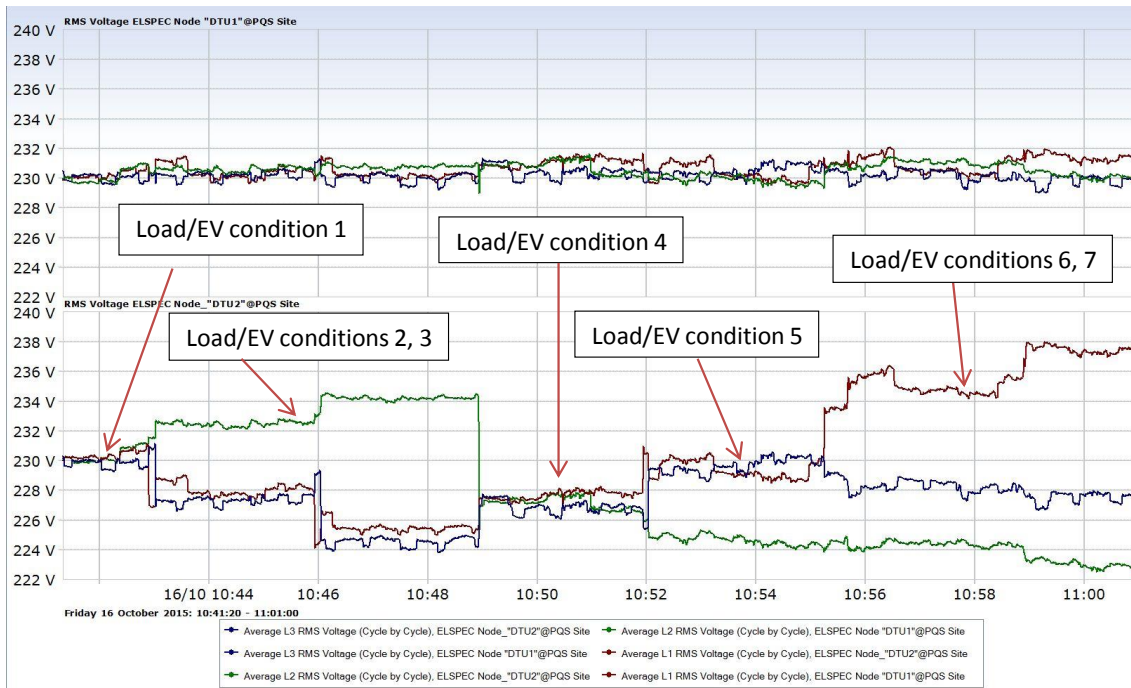| Load/EV condition	Phase a	Phase b	Phase c
1	0 kW	0 kW	0 kW
2	3.4 kW	0 kW	3.4 kW
3	6.7 kW	0 kW	6.7 kW
4	6.7 kW	6.7 kW	6.7 kW
5	3.4 kW	6.7 kW	3.4 kW
6	-1.8 kW (=-8 A @230V)	6.7 kW	3.4 kW
7	-3.7 kW (=-16 A @230 V)	6.7 kW	3.4 kW

7.2 Results of Control logics comparison

Fig. 54. Voltage measurement at OLTC bus and load/EV bus in the case of CL1

Fig. 54 shows the phase-neutral voltages at the two measurement points, in the scenario characterized by conventional OLTC operations CL1; i.e. considering local phase-neutral voltage measurements. It is noticed that, thanks to the tap-changing activities, the voltages at the OLTC or local bus (the controlled bus), are kept within the safe band. On the other hand, at the load/EV or remote bus they deviate unevenly from the rated value of 230 V, according to the grade of unbalance. Specifically, it can be noticed that the larger the difference of the three single-phase loads (see Table 14), the higher the deviations. It is also noticeable that the deviations decrease on the three phases, in correspondence to the balanced condition characterized by active power absorption of 6.7 kW on all phases (condition 4). Moreover, with regard to the most extreme conditions (6 and 7) — i.e., when the EV only injects current on one phase, while the other two absorb unevenly — the deviations are even more accentuated than for conditions 2 and 3, when the unbalance is obtained through different grades of loading on the three phases.
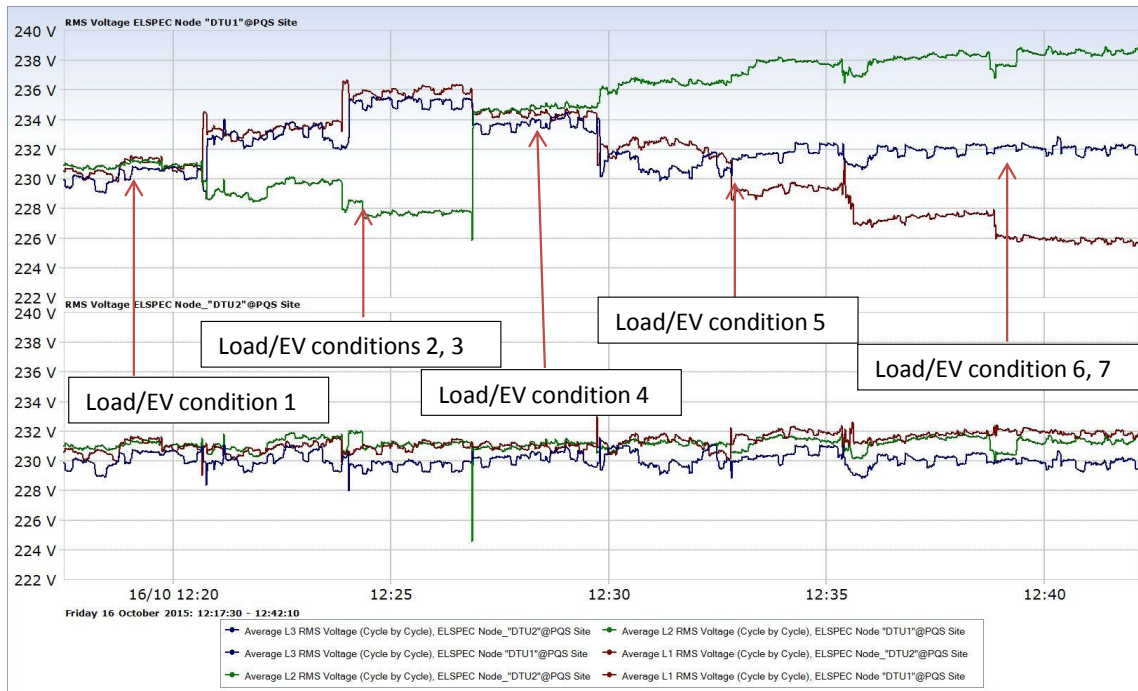
Fig. 55. Voltage measurement at OLTC bus and load/EV bus in case of CL2

Fig. 55 shows the phase-neutral voltages at the two measurement points, in the scenario characterized by OLTC operations based on phase-neutral measurements performed at the load/EV bus. It is noticed that the voltages at the load/EV bus (the controlled bus) are kept within the dead band, while on the other hand, at the OLTC bus, they deviate unevenly from the rated value of 230 V, according to the grade of unbalance. Basically, the situation is the reverse of the previous one, since the considered load/EV conditions are the same. The only difference is the measurement point, which is also the control objective, has been shifted from the local to the remote bus. Again, note that the larger the difference of the three single-phase loads, the higher the voltage deviations. It is also noticeable that the deviations are even on the three phases, in correspondence with the balanced condition characterized by the active power absorption of 6.7 kW on all phases (condition 4).

As explained in Paragraph 5.4, three stages are contained in the modified LDC control; i.e., CL4. To operate CL4 in real time, a pre-reference voltage setting of the tap changer is needed. Considering the various load/EV conditions defined in Table 13, Table 14 defines the position of the tap changer, which will be set before every change of the load/EV condition, with the purpose of counteracting the voltage change on each phase. The tap value is calculated based on (32) that uses the current learned from the experimental result of CL1.

$$n^{a,b,c} = \frac{\Delta V^{a,b,c}}{\Delta V_{step}} \tag{32}$$

A negative value in the table means an increase in the voltage at the secondary side of the OLTC, while a positive value means a decrease in the voltage.

Table 14. Definitive tap table used for CL4 in real-time operation

Load/EV condition	n^a	n^b	n^c
1	0	0	0
2	-2	1	-1
3	-4	2	-2
4	-2	-2	-2
5	0	-3	-2
6	3	-4	-3
7	4	-5	-3

With this table, at each step of the operation before changing the load/EV conditions, we change the tap changer preventively. The corresponding voltage profiles at the secondary side of the OLTC bus and the Load/EV bus are presented in Fig. 56.

Comparing Fig. 56 and Fig. 55, it is observed that CL4 keeps the voltage at the Load/EV bus in a similar band as the one presented in CL2. However, with this method the control of the voltage is not as precise as it was for the case presented by CL2. This may due to 1 (or 2) more tap positions on phase c, in the case of load/EV conditions 5, 6 and 7. Nevertheless, it presents and validates an approach for this type of on-load tap-changer transformer.
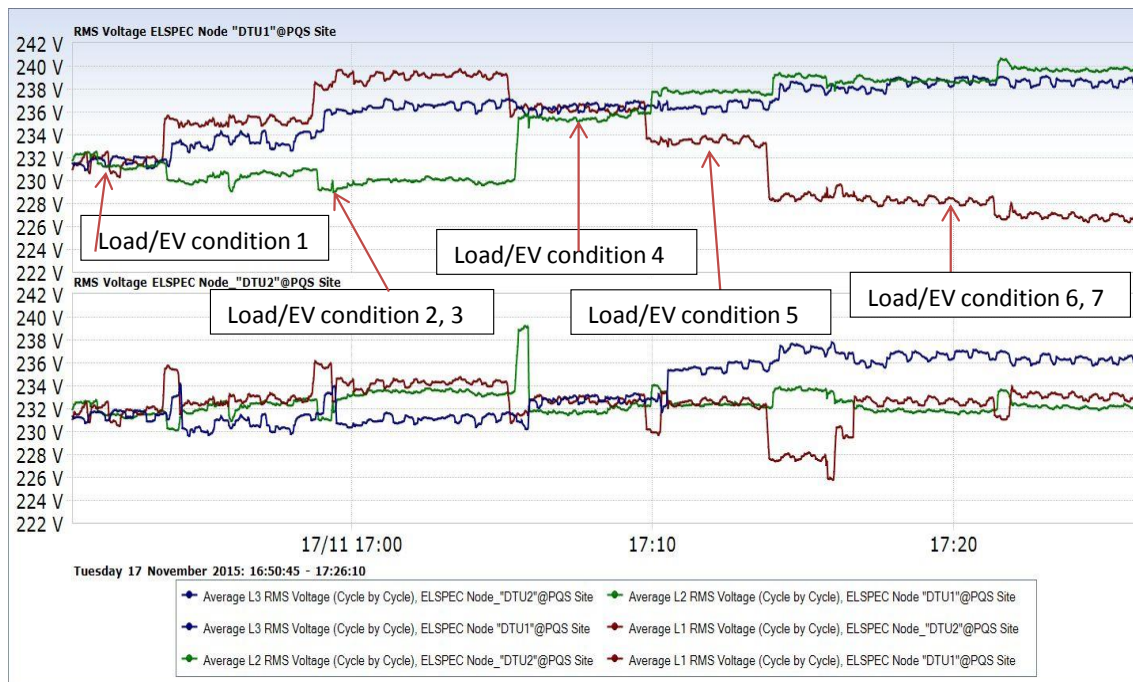

Fig. 56. Voltage measurement at OLTC bus and load/EV bus in case of CL4

As deduced from Table 15, in the case of CL1 and CL2, the deviations of the phase-neutral voltages to the correspondent reference value are kept within the voltage band at the controlled bus; i.e., at the local bus and remote bus, respectively. On the other hand, the uncontrolled bus is in both cases characterized by deviations up to 7.5 V in the case of Load/EV condition 7.

Regarding the CL4 scenario, as also shown in Fig. 56, the preventive tap position adjustment allows a reduction in the variation at the remote bus to maximum deviations of 2.6 and 1.8 V for phases a and b, respectively. On phase c it can be noticed that the deviation in the case of load/EV conditions 6 and 7 is a bit higher: 4.6 and 4.9 V, respectively. Although not perfectly matching the case CL2, the results indicate that this method is able to provide a good reduction of voltage variations at the remote bus, which in the case of traditional OLTC operations, based on local measurements (CL1), would have been drastically larger.

Table 15. Summary of phase-wise voltage profiles under three control scenarios

Scenario	Load/EV condition	Desired V a	$V_{meas}\,a$ local	$V_{meas}\,a$ remote	Desired V b	$V_{meas}\,b$ local	$V_{meas}\,b$ remote	Desired V c	$V_{meas}\,c$ local	$V_{meas}\,c$ remote
CL1	1	230.6 @local bus	230.2	230.3	230.5 @local bus	230.0	230.3	230.1 @local bus	230.0	229.8
	2		230.4	228.0		230.6	232.5		230.2	227.3
	3		230.2	225.5		230.8	234.2		230.0	224.5
	4		231.1	227.7		230.8	227.2		230.4	226.9
	5		230.4	229.4		229.9	224.6		230.4	229.6
	6		230.8	235.0		231.0	224.4		230.2	228.2
	7		231.4	237.4		230.1	223.0		229.8	227.5
CL2	1	231.2 @remote bus	230.8	230.9	231.2 @remote bus	230.9	231.0	230.1 @remote bus	230.2	230.1
	2		233.2	230.8		229.3	231.2		233.0	230.2
	3		235.9	231.0		227.7	231.2		235.2	229.7
	4		234.4	231.0		234.8	231.1		233.7	230.3
	5		232.3	231.4		236.5	231.2		230.9	230.1
	6		227.4	231.7		238.2	231.5		231.9	230.1
	7		225.9	231.9		238.5	231.3		232.1	229.9
CL4	1	231.6 @remote bus	231.6	231.7	231.6 @remote bus	231.6	231.8	231.7 @remote bus	231.7	231.5
	2		235.2	232.7		230.4	232.2		233.4	230.6
	3		239.1	234.2		230.0	233.4		236.5	231.1
	4		236.2	232.7		235.4	231.8		236.4	232.8
	5		233.5	232.6		237.7	232.4		236.5	235.6
	6		228.2	232.6		238.7	231.7		238.6	236.6
	7		226.8	233.1		239.7	232.1		238.6	236.3

8 CONCLUSIONS

This work presented both experimental and modeling activities of an OLTC transformer provided with single-phase-independent tapping capability, used to mitigate the increasing unbalanced conditions in distribution networks caused by the growing number of single-phase DERs.

Firstly, a detailed analysis aiming at a simplified representation of a real Danish LV distribution network is proposed: the obtained results allowed the choice of the components utilized for the tests, performed in the research infrastructure SYSLAB-PowerLabDK. Then, an investigation of the tap-changers' behavior has been carried out both in DIgSILENT PowerFactory software environment and in the lab environment. The comparison of the voltage trends showed that the proposed model in PowerFactory allows a realistic representation of the real tap operation. Additionally, the OLTC's operability is studied in two scenarios characterized by both balanced and unbalanced load conditions as well as single-phase reverse power flow. From the experimental tests, it can be concluded that at the transformer level voltages have been maintained within the dead band, confirming the effectiveness of the tap operations, being the OLTC based on local measurements.

Furthermore, three control logics were tested and compared in this study. The experimental test validates the control performance of the on-load tap changers. The study suggests that, using remote measurement (i.e., end of the LV feeder), the voltages of the system can be kept in a safe operational band by the OLTC transformer. However, this requires the availability of the remote measurement to the OLTC, which is an expensive upgrade. To resolve this problem, a proactive tap algorithm is defined to compensate the voltage drop and keep the voltage at the ending bus in a safe band.

It is noted that the system used in the study is a simplified network that cannot characterize all the features of a real distribution network, even though it is able to catch the most important ones. Future works could include two aspects: 1) investigate the OLTC's application in an active distribution network characterized by several subfeeders, where higher penetration of different distributed generations is present; in such a case, the voltage rise/drop estimation may need some rethinking; and 2) combine the OLTC control with smart-metering technology, where the measurements from the smart meters can be used as inputs for the OLTC transformer.

REFERENCES

[1]   E. Caamaño-Martín, H. Laukamp, M. Jantsch, T. Erge, J. Thornycroft, H. De Moor, S. Cobben, D. Suna, and B. Gaiddon, "Interaction between photovoltaic distributed generation and electricity networks," *Prog. Photovoltaics Res. Appl.*, vol. 16, no. 7, pp. 629–643, 2008.

[2]   M. Braun, T. Stetz, R. Bründlinger, C. Mayr, K. Ogimoto, H. Hatta, H. Kobayashi, B. Kroposki, B. Mather, and M. Coddington, "Is the distribution grid ready to accept large-scale photovoltaic deployment? State of the art, progress, and future prospects," *Prog. photovoltaics Res. Appl.*, vol. 20, no. 6, pp. 681–697, 2012.

[3]   T. Stetz, M. Kraiczy, M. Braun, and S. Schmidt, "Technical and economical assessment of voltage control strategies in distribution grids," *Prog. Photovoltaics Res. Appl.*, vol. 21, no. 6, pp. 1292–1307, 2013.

[4]   K. Knezovic, M. Marinelli, R. J. Moller, P. B. Andersen, C. Traholt, and F. Sossan, "Analysis of voltage support by electric vehicles and photovoltaic in a real Danish low voltage network," in *Power Engineering Conference (UPEC), 49th International Universities, Cluj-Napoca, Romania*, 2014, pp. 1–6.

[5]   J. Hu, S. You, M. Lind, and J. Østergaard, "Coordinated charging of electric vehicle for congestion prevention in the distribution grid," *IEEE Trans. smart grids*, vol. 5, no. 2, pp. 703–711, 2014.

[6]   D. Johnston, "On-Line Independent Tap-Changing of Each Feeder Supplied by a Low Voltage Distribution Transformer," *J. Power Energy Eng.*, vol. 2, no. April, pp. 388–394, 2014.

[7]   N. Efkarpidis, C. Gonzalez, T. Wijnhoven, D. Van Dommelen, T. De Rybel, and J. Driesen, "Technical Assessment of On-Load Tap-Changers in Flemish LV Distribution Grids," *3rd Int. Work. Integr. Sol. Power into Power Syst.*, 2013.

[8]   M. Coppo, R. Turri, M. Marinelli, and X. Han, "Voltage Management in Unbalanced Low Voltage Networks Using a Decoupled Phase-Tap-Changer Transformer," in *Power Engineering Conference (UPEC), 2014 49th International Universities, Cluj-Napoca, Romania*, 2014, pp. 1–6.

[9]   A. Zecchino, M. Marinelli, J. Hu, M. Coppo, and R. Turri, "Voltage Control for Unbalanced Low Voltage Grids Using a Decoupled-Phase On-Load Tap-Changer Transformer and Photovoltaic Inverters," *Proceedings of UPEC 2015*. IEEE, Stoke-On-Trent, 2015.

[10]   J. Hu, M. Marinelli, M. Coppo, A. Zecchino, and H. W. Bindner, "Coordinated voltage control of a decoupled three-phase on load tap changer transformer and photovoltaic inverters for managing unbalanced networks," *Electr. Power Syst.*

Res., vol. 99, 2015.

[11]   "SYSLAB-PowerLabDK." .

[12]   ELSPEC, "G4500 & G3500 Portable Power Quality Analyzer USER & INSTALLATION MANUAL." V1.2 SMX-0618-0100, 2013.

[13]   "IEEE Task Force on Load Representation for Dynamic Performance, Load representation for dynamic performance analysis," *IEEE Trans. Power Syst.*, vol. 8, no. 2, pp. 472–482, 1993.

[14]   S. Martinenas, M. Marinelli, P. B. Andersen, and C. Træholt, "Implementation and demonstration of grid frequency support by V2G enabled electric vehicle," *Proc. 49th Int. Univ. Power Eng. Conf. IEEE, Cluj- Napoca Rom.*, pp. 1–6, 2014.

[15]   T. Gonen, "Electric power distribution engineering." CRC Press, 2014.

[16]   F. A. Viawan, A. Sannino, and J. Daalder, "Voltage control with on-load tap changers in medium voltage feeders in presence of distributed generation," *Electr. Power Syst. Res.*, vol. 77, no. 10, pp. 1314–1322, Aug. 2007.

[17]   P. Pillay and M. Manyage, "Definitions of Voltage Unbalance," *IEEE Power Eng. Rev.*, pp. 50–51, 2001.

www.elektro.dtu.dk/cee